

# Fluid Velocity Vector Field Measurement in Synovial Joints

A THESIS PRESENTED  
BY  
LAURA S. MORTIMER  
TO  
THE DEPARTMENT OF MECHANICAL ENGINEERING  
IN PARTIAL FULFILLMENT OF THE REQUIREMENTS  
FOR THE DEGREE OF  
MASTER OF MECHANICAL ENGINEERING  
IN THE SUBJECT OF  
MECHANICAL ENGINEERING  
SAINT MARTIN'S UNIVERSITY  
LACEY, WASHINGTON  
DECEMBER 2017

---

Laura S. Mortimer, M.M.E. Candidate

---

Date

---

Frank M. Washko, Ph.D., J.D., Thesis Committee Chair

---

Date

---

Shawn Duan, Ph.D., Department Chair, Examiner

---

Date

---

Rico A.R. Picone, Ph.D., Examiner

---

Date

©2017 – LAURA S. MORTIMER  
ALL RIGHTS RESERVED.

## Fluid Velocity Vector Field Measurement in Synovial Joints

### ABSTRACT

The movement of the human knee during flexion and extension is difficult to model due to the complicated motion of simultaneous rotation and sliding. Little research has been done on synovial joints such as the knee and their lubrication and wear capabilities. A Particle Image Velocimetry system was used to demonstrate the capability to investigate the velocity of the fluid in a knee model for both extension and flexion. The positive feedback of the demonstration to incorporate Particle Image Velocimetry within the biomechanics industry will help to improve the lifespan of various implants and the accuracy of many surgeries.

# Acknowledgments

I would like to thank my husband Ronald Boursaw Jr. for his love, support, and constant motivation throughout the length of this process.

I would like to thank my parents, Chuck and Sue Mortimer for their continuous support and encouragement in everything I do.

I would also like to thank my advisor, Dr. Frank Washko, and professor, Dr. Rico Picone, for their help and guidance with this project and my career at Saint Martin's University.

# Contents

0	INTRODUCTION	7
1	BACKGROUND	10
1.1	The Human Knee . . . . .	10
1.2	Sliding Bearings and Lubrication . . . . .	13
2	TESTING HARDWARE	19
2.1	Particle Image Velocimetry . . . . .	19
2.2	Testing equipment . . . . .	22
2.3	Testing parameters . . . . .	25
3	DATA	27
4	ANALYSIS	55
4.1	Extension . . . . .	55
4.2	Flexion . . . . .	58
5	CONCLUSION	62
	REFERENCES	66

# Listing of tables

3.1	corresponding figures . . . . .	28
4.1	Extension Data . . . . .	56
4.2	Flexion Data . . . . .	59

# Listing of figures

1	Diagram of Knee Movement . . . . .	8
1.1	Anatomy of the Human Knee . . . . .	11
1.2	Lubrication in articular cartilage . . . . .	14
1.3	pressure wedge . . . . .	15
1.4	models currently in use . . . . .	17
1.5	Area of Interest . . . . .	18
2.1	Basic PIV set-up . . . . .	20
2.2	Sawbones Purchased Model . . . . .	23
2.3	Test Set-Up . . . . .	25
3.1	Extension area orientation . . . . .	29
3.2	Flexion area orientation . . . . .	29
3.3	1 rad/s Before Completeing Extension . . . . .	30
3.4	1 rad/s Before Completeing Extension Over Raw Image . . . . .	31
3.5	1 rad/s Before Completeing Extension Velocity Only . . . . .	32
3.6	1 rad/s After Completeing Extension . . . . .	33
3.7	1 rad/s After Completeing Extension Over Raw Image . . . . .	34
3.8	1 rad/s After Completeing Extension Velocity Only . . . . .	35
3.9	3 rad/s Before Completeing Extension . . . . .	36
3.10	3 rad/s Before Completeing Extension Over Raw Image . . . . .	37
3.11	3 rad/s Before Completeing Extension Velocity Only . . . . .	38
3.12	3 rad/s After Completeing Extension . . . . .	39
3.13	3 rad/s After Completeing Extension Over Raw Image . . . . .	40
3.14	3 rad/s After Completeing Extension Velocity Only . . . . .	41
3.15	1 rad/s Before Completeing Flexion . . . . .	42
3.16	1 rad/s Before Completeing Flexion Over Raw Image . . . . .	43
3.17	1 rad/s Before Completeing Flexion Velocity Only . . . . .	44
3.18	1 rad/s After Completeing Flexion . . . . .	45
3.19	1 rad/s After Completeing Flexion Over Raw Image . . . . .	46
3.20	1 rad/s After Completeing Flexion Velocity Only . . . . .	47
3.21	3 rad/s Before Completeing Flexion . . . . .	48
3.22	3 rad/s Before Completeing Flexion Over Raw Image . . . . .	49
3.23	3 rad/s Before Completeing Flexion Velocity Only . . . . .	50

3.24	3 rad/s After Completeing Flexion . . . . .	51
3.25	3 rad/s After Stopping Completeing Over Raw Image . . . . .	52
3.26	3 rad/s After Stopping Completeing Velocity Only . . . . .	53
4.1	Slow Flexion Vorticity . . . . .	61
5.1	Illustration of the Burmester curve and four-bar linkage system . . . . .	64

# 0

## Introduction

Synovial joints can be modeled as sliding bearings due to their similar lubrication methods. Sets of equations and experimental graphs to determine such values as load bearing capacity, friction, and wear between the two surfaces already exist. In the case of the knee, the two bearing surfaces of the femoral condyles and the tibial plateau both slide and rotate at the same time. This type of movement, which can be seen in Figure 1 below, can not be modeled in the same way as other synovial joints.

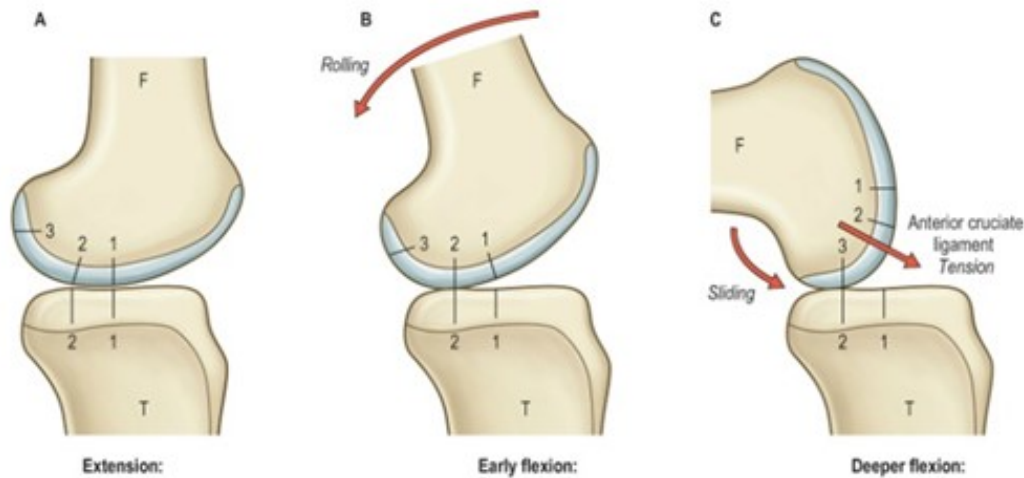


Figure 1: Diagram of Knee Movement [21]

Due to the complicated motion, minimal literature exists on the movement of the synovial fluid and conditions of the bearing surfaces in the human knee.

One of the more advanced techniques for studying and measuring fluid velocity and movement is Particle Image Velocimetry (PIV). This system uses a planar laser and a camera to track the movements of seeded particles in a fluid. Typically, this technology is used with wind tunnels and large-scale objects such as airplane wings. Typically, confined spaces are not used with PIV technology. This thesis analyses the feasibility of using this technology on a physical test model to determine synovial fluid velocity vectors.

This type of research into the fluid movement in the knee has the potential to lead to a better understanding of the joint and the hopeful correlation to a Computational Fluid Dynamic (CFD) model. Once a working CFD model is achieved, we can begin to understand how the fluid movement affects rehabilitation

of swollen joints, knee surgeries, and implants. This same model could be used to determine the optimal geometry for implants and cartilage grafts for the best-case wear or load carrying performance. Injection points for drugs into joints could also be optimized as the model could be used to study the migration of the drug into the joint.

# 1

## Background

### 1.1 THE HUMAN KNEE

The human knee joint is encompassed by three main bones; the femur(thigh bone), the tibia (shinbone), and the patella (kneecap). The joint also contains ligaments, tendons, and a meniscus. The ligaments join the bones to provide stability and constrain the bones to prevent them from sliding too far in any direction. Tendons help provide motion transfer from the muscles to bones. The meniscus is

broken into two pieces, the lateral and medial meniscus, and is located at the top of the tibia to act as a shock absorber in the joint and the bearing surface. These cartilage disks help to protect an even more important piece of cartilage - the articular cartilage. This thin layer surrounding the bottom of the femur allows the bones to slide and rotate about each other with minimal friction. Biomechanical properties in the articular cartilage are a strong player in typical knee joint function. The compressive load bearing properties of the articular cartilage in the knee are directly dependant on the cartilage and synovial fluid interaction [2]. This cartilage can be easily damaged and torn and therefor has to be replaced as a common procedure. Figure 1.1 below shows the anatomy of the human knee.

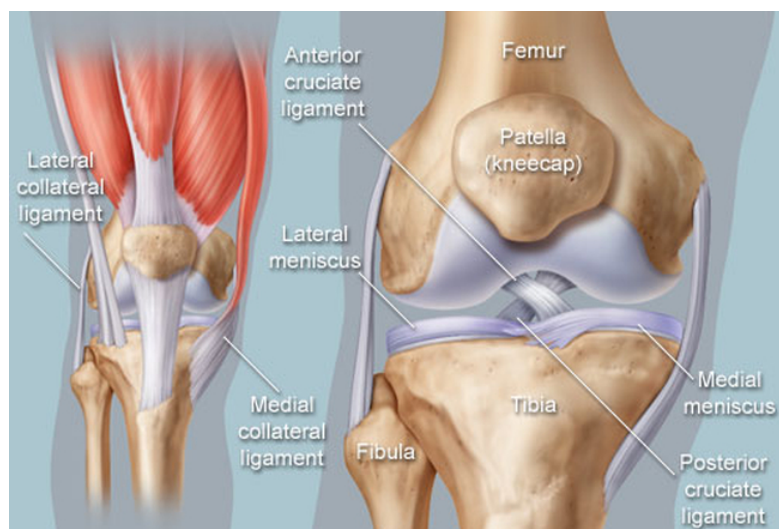


**Figure 1.1:** Anatomy of the Human Knee [8]

The capsule containing the synovial fluid around the knee consists of a synovial membrane and a fibrous sleeve [17]. This membrane is attached around the articular surfaces of the femur and tibia. This capsule of fluid helps lubricate the bearing surfaces of the bones to reduce friction and wear. Synovial

joints are expected to last the lifetime of the human body while transmitting large dynamic loads and accommodating a range of various movements [10]. Joints such as the knee go through various loading conditions during common activities such as walking, running, stretching, and even standing. During strenuous movements, the hip and knee joints can see contact pressures of up to 18 MPa [12]. These stresses on the articular cartilage can cause degeneration which will lead to the need of cartilage replacements. Boundary lubrications in the joints have a huge impact on the wear of cartilage and the friction conditions of cartilage replacement materials have been researched extensively. The known nature of articular cartilage contributes to its high load bearing capacity. When a load is applied, the interstitial fluid pressurization increases almost instantaneously which leads to a high fluid phase load in the cartilage [12]. The materials used as a replacement for the cartilage dictates how high the pressures will get. Unfortunately, it is difficult to accurately measure the fluid motion in the knee while simulating realistic motion.

Previous studies on the human knee have investigated various types of friction and wear of the articular cartilage. In cartilage, low friction and low wear rate are important characteristics and are controlled by the lubricant which adapts to the changing loads and sliding rates during motion. A study done in Germany in 2015 found that a low friction coefficient between the articular cartilage and the lubricating fluid does not correlate with low wear [13]. The presence of hyaluronic acid in the synovial fluid does not affect the friction coefficient, but does significantly reduce wear in the knee [13]. This information is helpful in determining a proper lubrication to be used in knee replacements and surgeries.

In 2015, a study was done on compressive loads in the human joint. The research done targeted the

medial and lateral meniscus and used CT scans from a volunteer to calculate 3D surfaces and convert them to CATIA files [15]. Load bearing conditions were assumed at a sturdy standing condition and stresses were calculated while taking into account Young's modulus for the different materials in the joint. This finite element analysis proved useful in determining which meniscus saw higher stress but didn't take into account any type of movement.

The movement in the human knee is difficult to model as stated previously. Currently, the majority of knee reconstructive surgeries are performed arthroscopically for minimal invasiveness [7]. This leads to minimal visibility of the complex knee anatomy and its workings. When working with total knee replacements, simple models have been used, such as a multi directional tribological system, to test replacement technologies. These systems resemble a half sphere sliding and rolling on a disk. This custom ball-on-flat systems can be seen in Figure 1.4. It is estimated that 9% of total knee arthroplasty procedures require revision surgeries down the road [18] and the bearing components of many hip prostheses can separate up to 2 mm in the body during typical exercises as walking [20]. This statistic is caused by the limited information on how replacements will wear over time.

## 1.2 SLIDING BEARINGS AND LUBRICATION

The most common model for synovial joints such as the knee is a sliding bearing. A sliding bearing, sometimes called an antifriction bearing, consists of a shaft or journal rotating or oscillating within a sleeve with the main motion being sliding or rolling. A liquid is inserted between the two surfaces in order to reduce friction, wear, and heating of the parts [3]. There are a variety of lubrication types used

in bearings or when looking at articular cartilage. The figure below shows the five types of lubrication of articular cartilage in joints such as the knee.

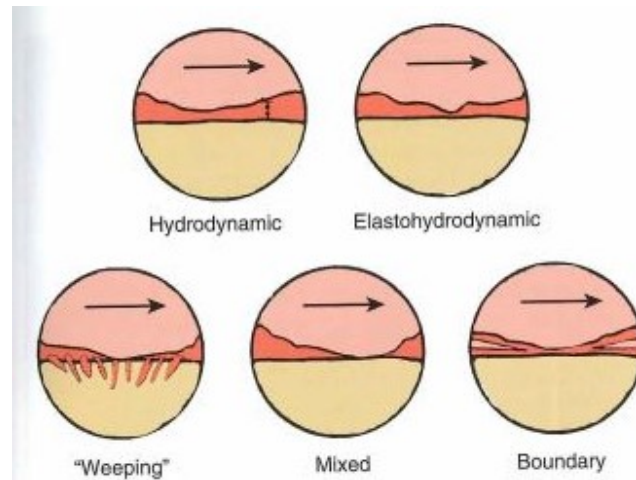


**Figure 1.2:** Lubrication in articular cartilage [16]

The distinct form of sliding lubrication typically used in association with synovial joints and articular cartilage is typically hydrodynamic lubrication. Hydrodynamic lubrication, is when the load-bearing surfaces are separated by a thick film of lubricant, such as the capsule of synovial fluid in a knee. The pressure in the lubricant are created by the moving surfaces pulling the fluid around into typically wedge shaped zones [3]. Figure 1.3 below shows a diagram of a bearing lubrication pressure wedge.

The knee could potentially be modeled as boundary lubrication, or thin film lubrication, bearing due to the possibility of there not being enough fluid around the meniscus and contact being made. For this investigation, the model was looked at as a hydrodynamic bearing. When looking at sliding bearings and hydrodynamic lubrication, some assumptions are made. It is assumed that the fluid film flow is laminar at a low Reynolds number ( $Re$ ). This value is used as an estimate of the ratio

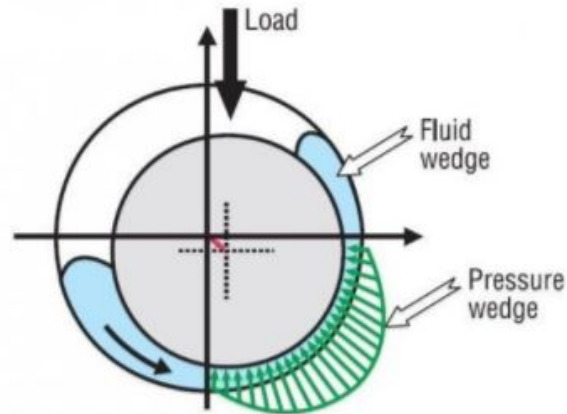


Figure 1.3: Pressure wedge in bearing [1]

of the inertial and viscous forces in a fluid. The liquid used as the lubricant is also assumed to be incompressible and have a linear relationship between the stress and strain rate [6]. Although machined hydrodynamic bearings are a close representation of a synovial joint, the cartilage and synovial fluid are considered to be superior in friction performance when compared to any manmade bearing [6].

The flow of all lubricants follow the basic laws of fluid dynamics. Specifically, conservation of mass and the Navier-Stokes equations for conservation of momentum are followed while assuming incompressible flow in the lubrication. One of the important characteristics in lubrication theory is the viscosity of the lubricant. The viscosity is a constant of proportionality and a measure of the internal frictional resistance of the fluid [3]. Viscosity is sensitive to small temperature changes thus making bearing temperature a key factor in bearing design [6]. The other three important design considerations of a sliding bearing are the load per unit of projected bearing surface, the speed of the motion, and the bearing physical dimensions. The dependent variables, also known as the performance factors, are the coefficient of

friction, the volumetric flow rate, and the minimum film thickness in a sliding bearing [3].

To be able to analyze a hydrodynamic bearing, the velocity of the lubrication must be known. The velocity, or even the volumetric flow rate, of the fluid at the boundary layer between the fluid and solid bearing wall is of critical interest. The velocity gradient directly correlates with the forces and stressing put along the bearing surface [6]. The velocity of the bearing surface is important as well since the first layer of fluid in the bearing will have the same velocity. The drag force that occurs directly inside of the bearing surface is dependant on the volumetric flow rate and the viscosity of the fluid. The friction behavior in a bearing depends on the dynamic viscosity of the fluid, the relative velocity, and the load per seen in the projected are [5]. When it comes to synovial joints, there is very little understanding of what the volumetric flow or velocity is in the fluid.

The traditional lab testing machines and simulators for joints in use today are useful in analyzing the basic components in a joint such as material on material wear, but lack the complex motion actually occurring in the joint. A study done on ultra-high molecular weight polyethylene bearing components with knee replacements explains that there is minimal literature on any type of lab wear tester that can simulate both cross shear sliding and rolling-sliding motion, and both play a key factor in the stress state of the knee [18]. Complex models of the knee do exist, but specific aspects and stress states can't be isolated to analyze. Figure 1.4 below shows various types of models currently in use to test knee replacement materials.

Some research has been done on sliding bearings in regards to surface texturing. According to a study done in 2013, partial texturing and partial slip pattern on the actual bearing surfaces help to

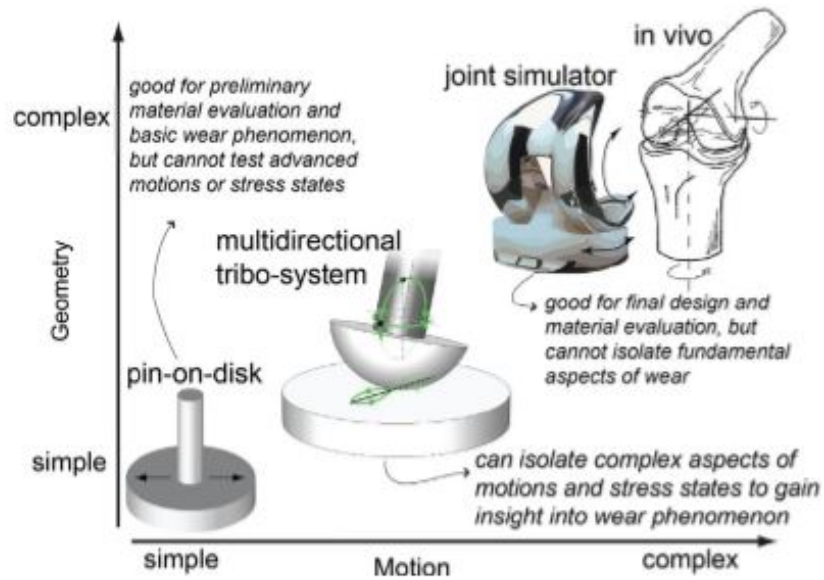


Figure 1.4: models currently in use [18]

reduce friction and increase the load support in the joint [19]. This will improve the performance in hydrodynamic bearings.

The area of interest for this project is the triangle shape of fluid between the femoral condyle, the tibial plateau, and the patella/patellar tendon that can be seen when looking at a knee from the side. This area will give insight to the velocities and direction of the fluid entering or leaving the bearing surface in the synovial joint. An x-ray showing our area of interest can be found in Figure 1.5 below.



Figure 1.5: Area of Interest [9]

# 2

## Testing Hardware

### 2.1 PARTICLE IMAGE VELOCIMETRY

PIV test systems are made of 3 main components; a laser, a camera, and a programmable timing unit to control them. The typical set-up is documented in the schematic below [11]. Two different laser beams are pulsed through a cylindrical lens that converts the light into a sheet that will illuminate particles in the fluid of interest. The camera will in turn take multiple snapshots that will show the locations and

movements of these individual particles. Various image processing programs can be applied to track movement of these particles. For this investigation, LaVision equipment was used alongside with their DaVis software to record and analyze various data sets. The main goal of a PIV system is to track the velocity of fluid particles at various times and locations. One major strength of PIV technology is its range of flows that it can be used with. Both liquids and gases in various amounts can be used with PIV as long as the medium is transparent with optical access for the camera to see into. The spatial resolution of PIV is also flexible which helps to increase the strengths of this form of fluid measurements [11].

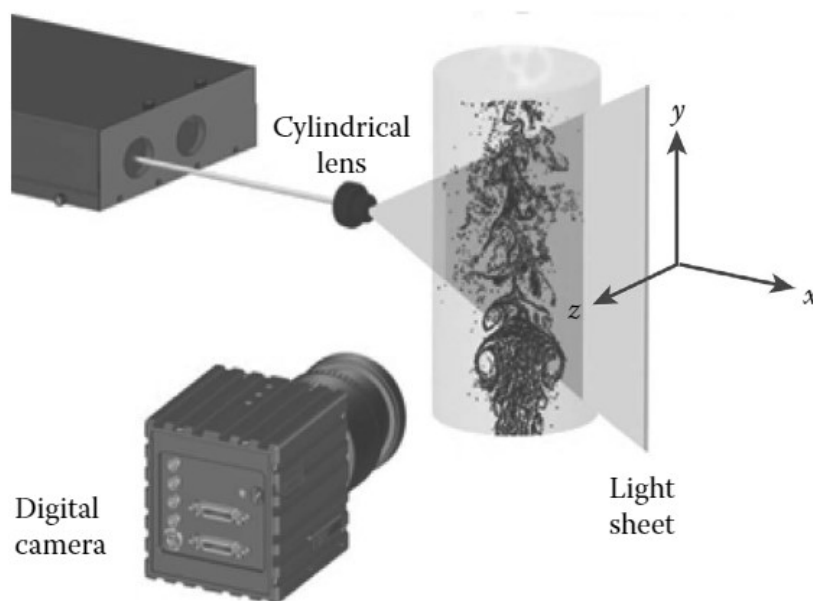


Figure 2.1: Basic PIV set-up [11]

When collecting data using a PIV system, each measurement is formed by a pair of images with a

designated time difference between them. This time difference is typically selected based on the capabilities of the laser timing from the specific unit. These images are taken using greyscale digital images so that it is easy to systematically assign binary values to the pixels in each image. These pixels represent image spatial units and this binary units are used to track movement using a process called “spatial cross-correlation”. This method returns the most likely vector that matches with various pixels in a specific interrogation region in the form of a grid [11]. During postprocessing, a vector is computed for every grid location and the “bad vectors” are removed and missing data is assumed to create a full picture of the movement being tracked. A reference measurement must be including during postprocessing so that accurate velocities are being computed. Other settings that help to collect useful data using a PIV system is different spatial resolutions and different bit depths. These options can be dictated to the software before collecting data in hopes of capturing useful images.

An additional factor in collecting useful data is the selection of the tracer particle to be used in the fluid. These particles can be different sizes and added into the fluid in different densities. These particles must be naturally buoyant so that they will follow the flow during movement. Different seed particles are used between liquids and gasses. For the tests being ran in this investigation, fluorescent particles of about 40 microns in diameter were used as tracers. These particles are best used when dealing with solid surfaces around the fluid area. These specific particles take the incident light from the laser (532nm wavelength) and shifts the wavelength when hitting the particles to a higher wavelength [11]. Fluorescent particles tend to be more expensive than other tracer particles and therefore are only used in small scale fluid applications. These particles help the postprocessing software to track the fluid

velocities.

Traditional PIV technology is rarely used in small, confined, and enclosed fluid spaces due to the difficulty in fluid management, sight into the area of interest, and the complexity of the set ups. When it comes to flows, ventilation systems, large tubes, and the flow around plane turbines are the most common analyzed using PIV technology. The general dimensions for a small-scale model to be used with PIV matches up with the field of view. A comparison for a PIV system vs. a mini PIV system shares that a general field of view for our unit is roughly 0.15 m by 0.13 m [4]. Typically, it is difficult to model enclosed spaces due to the limitation of visibility into the area of interest. Very little research has been done with PIV technology on enclosed spaces and the introduction of this technology into the biomechanical field is a new area of research as well.

## 2.2 TESTING EQUIPMENT

For this project, a LaVision FlowMaster PIV system consisting of a VZ-Trigger Programmable timing unit, a 532 nm EverGreen MJ Laser and cooling system, and Nikon Camera lenses were used and paired with Davis 8.4 image processing software.

To look at the fluid movement in the human knee, a set-up was constructed using many different components. The base knee model is a clear acrylic Sawbones 1701-267 knee joint which is typically used as a model in doctors offices. The purchased model uses elastic bands and cords to simulate the collateral and cruciate ligaments. Figure 2.2 below shows the model that was purchased for this

investigation. The most important aspect when selecting a knee model was the inclusion of a clear patella for the laser to be able to go into the area of interest.



**Figure 2.2:** Sawbone Purchased Model

A thin sheet of silicone rubber, 0.010" thick with a 20a durometer, was wrapped around the joint and joined together by Room Temperature Vulcanization silicone (RTV) to simulate the synovial capsule and contain the fluid. The rubber was cut and joined to the clear patella by RTV in a similar fashion as a knee brace. Two two-inch diameter clear acrylic rounds were added into the sack at the area of interest. One acrylic round was attached directly to the side of the Femur to help keep the viewing round, which was RTV'd to the rubber sac, at a consistent angle for clear data. Both the top and

bottom of the synovial capsule were closed by multiple sealing bands.

The sack around the joint was filled with a water based test fluid that contained fluorescent particles approximately 40 microns in diameter that fluoresce pink under the wavelength of 532nm coming from our laser. De-ionized water was first heated and combined with Tween20 surfactant at a specific ratio of .10 grams surfactant per 100ml of water. This solution is then mixed with the microbeads at a ratio of 2.0ml liquid to 0.5g microbeads and mixed for approximately 10 minutes to get the spheres wetted into the solution. The mixture was then injected by needle into the simulated synovial capsule at the top.

A four-inch stroke actuator was mounted to the femur to simulate both extension and flexion of the knee. The specific model from Progressive Automation used was PA-15-4-11 4-inch actuator and calls for 12 Volts DC and has a force of 11 lbs which translates to approximately .17 m/s. The actuator was attached to the top of the femur on the model as well as a wood base to hold it up. Both the wood base and the knee model were then attached to the testing table.

The laser was set up directly in line behind the actuator stand so that the laser would put out a sheet along the sagittal plane and penetrate our model directly through the patella. The camera pointed at the side of knee through the clear viewing round, or along the frontal axis, at approximately 90 degrees from the line of sight of the laser. Figure 2.3 below shows the entire set-up.



Figure 2.3: Test Set-Up

### 2.3 TESTING PARAMETERS

Four different cases were tested with the current set-up; slow extension, fast extension, slow flexion, and fast flexion. To simulate a slow movement, 12 volts were used with the actuator which resulted in

an actuation velocity of roughly .17 meters/sec and a rotational speed of the knee of about 1 rad/s. For the faster motion, 24 volts were ran through the actuator resulting in an actuation velocity of roughly .5 meters/sec and a rotation speed of about 3 rad/s. For comparison, the average max rotational velocity of the adult human knee when going from a sitting position to standing is 2.6 rad/s [14]. When attempting to record the movement of the joint, it was noted that the viewing area would move out of the camera's frame due to the type of motion. This meant that the full extension or flexion could not be captured. In each case, the end result was kept in the frame resulting in the final moments of the physical movement and what happens when the movement stops. A trigger rate of 15 Hz was selected for image capturing and the time between laser pulses selected was 6000  $\mu$ s.

# 3

## Data

The system above was ran, and a variety of data points were taken. For each specific set up, a video was taken with the camera stationary at the end result of the motion. From this series of image pairs, two specific moments were analyzed; the fluid movement approximately  $1/15$ th of a second before the extension or flexion was completed and the fluid movement just after stopping the extension or flexion.

Using the LaVision image processing software, the fluescent particles were tracked. For the following

figures in this chapter, three images were recorded. The first figure with the white background shows the direction of the fluid with small black arrows. The arrows are overlaid on a colored diagram of the area of interest representing the vorticity of the fluid. This figure is helpful in pointing out any areas of circular motion and the general idea of where the fluid is going. The second figure for each image with the dark background is the raw image from the camera with velocity arrows overlaid. In this figure, the arrows are colored to indicate the velocity of the specific particles are moving. The third image for each data point also is used to see the velocity gradient. The colored area of interest depicts the velocity magnitude while the black arrows show direction. The table below summarizes the corresponding images with the 4 specific set ups.

Set up	Rotational Speed	When	Corresponding Figures
1	1 rad/s	Near the end of Extension	3.3, 3.4 , 3.5
1	1 rad/s	Immediately after completeing Extension	3.6, 3.7 , 3.8
2	3 rad/s	Near the end of Extension	3.9, 3.10, 3.11
2	3 rad/s	Immediately after completeing Extension	3.12, 3.13 , 3.14
3	1 rad/s	Near the end of Flexion	3.15, 3.16 , 3.17
3	1 rad/s	Immediately after completeing Flexion	3.18, 3.19, 3.20
4	3 rad/s	Near the end of Flexion	3.21, 3.22, 3.23
4	3 rad/s	Immediately after completeing Flexion	3.24, 3.25 , 3.26

**Table 3.1:** corresponding figures

For the extension data and images, the area analyzed is roughly a triangle between the tibia, femur, and patella. Figure 3.1 below helps to depict the orientation of the knee and area of interest at the time the data was collected. For the flexion data, the same triangle area was analyzed but is shaped differently. Figure 3.2 below helps to depict the orientation.

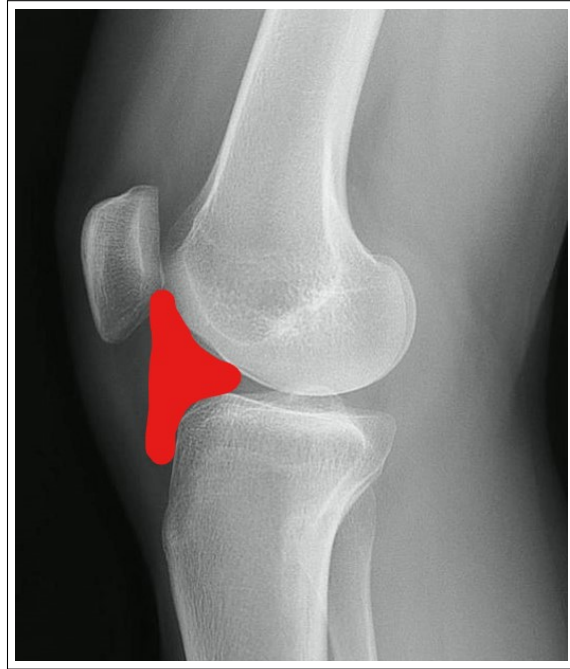


Figure 3.1: Extension area orientation [9]



Figure 3.2: Flexion area orientation [9]

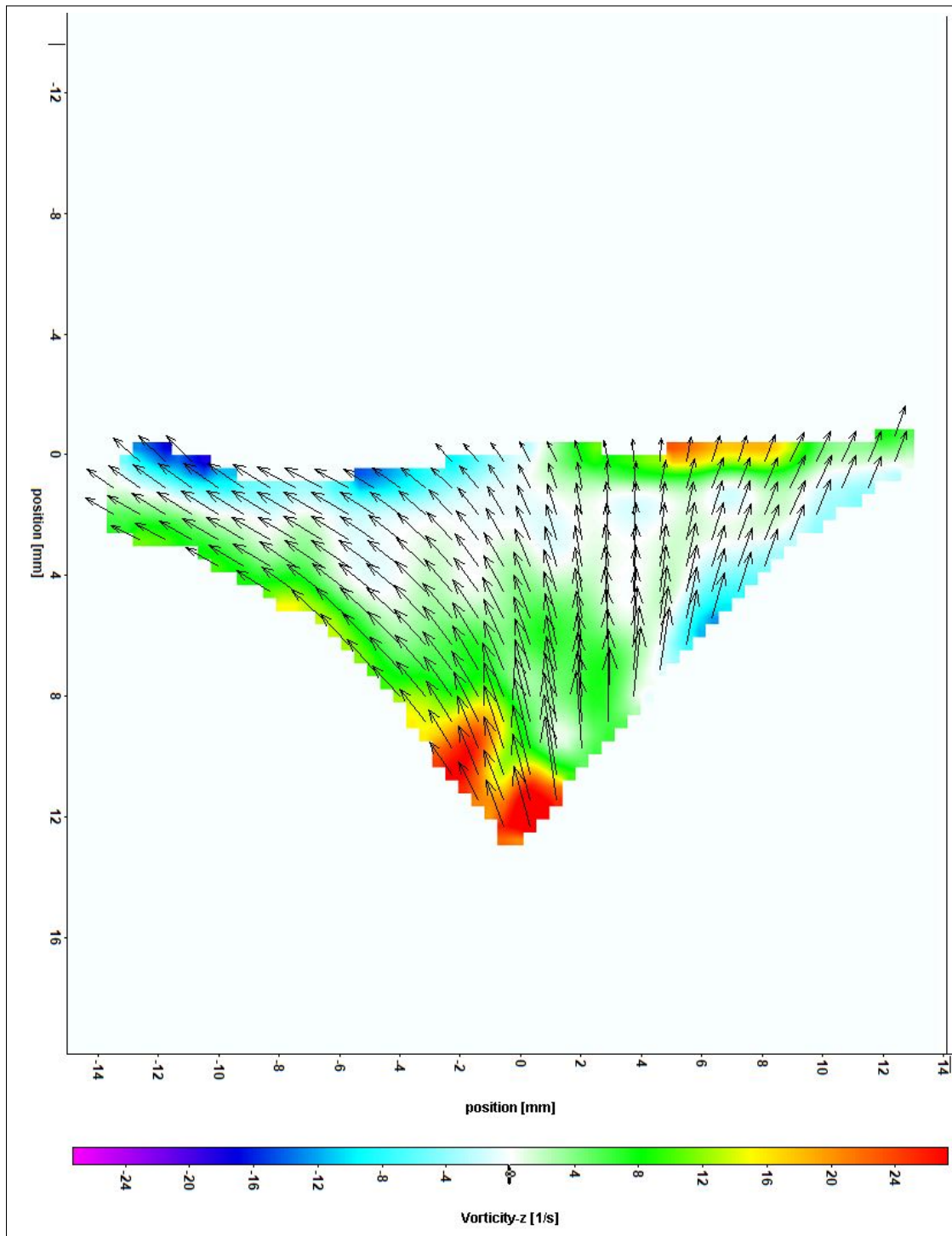


Figure 3.3: 1 rad/s Before Completing Extension

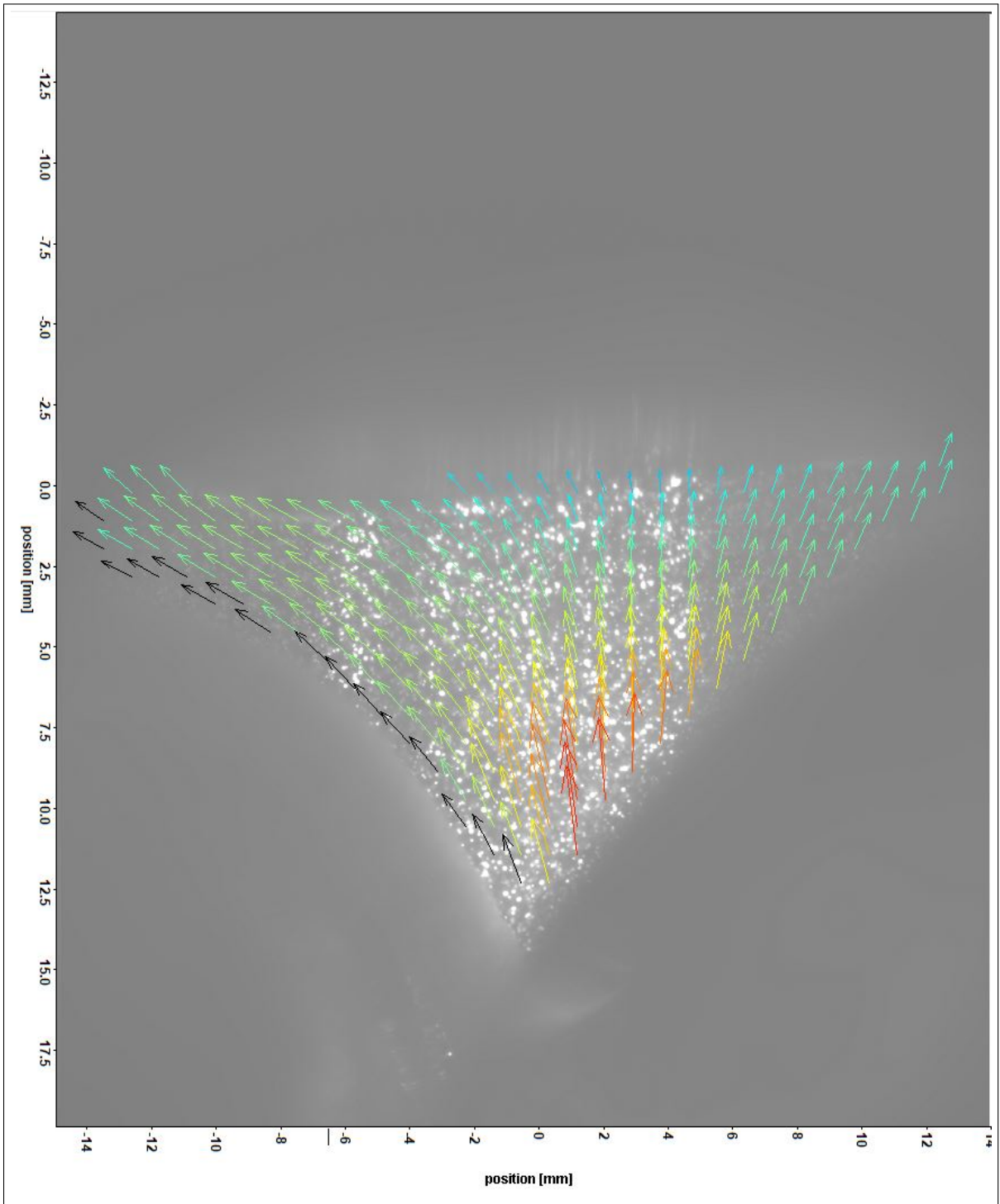


Figure 3.4: 1 rad/s Before Completing Extension Over Raw Image

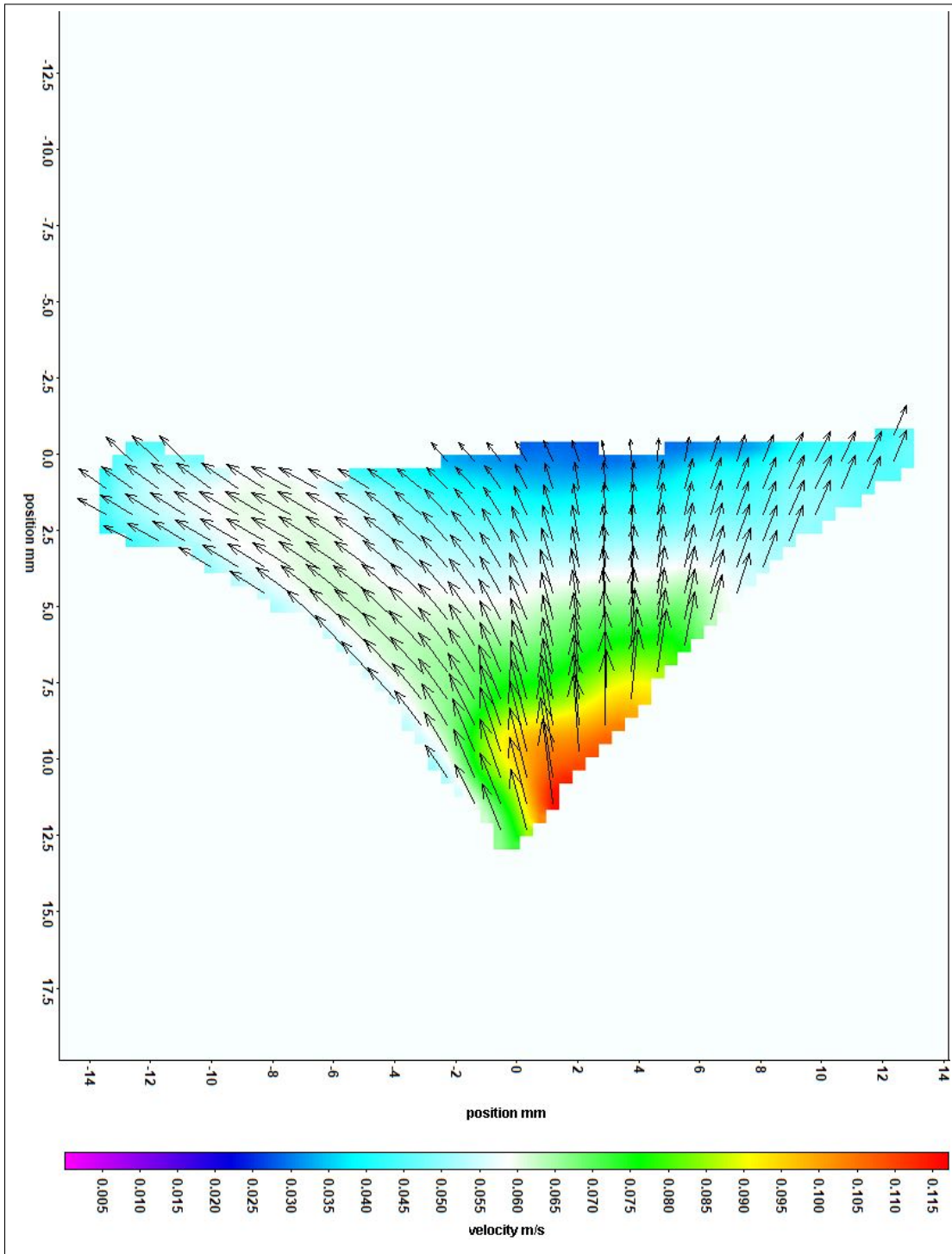


Figure 3.5: 1 rad/s Before Completing Extension Velocity Only

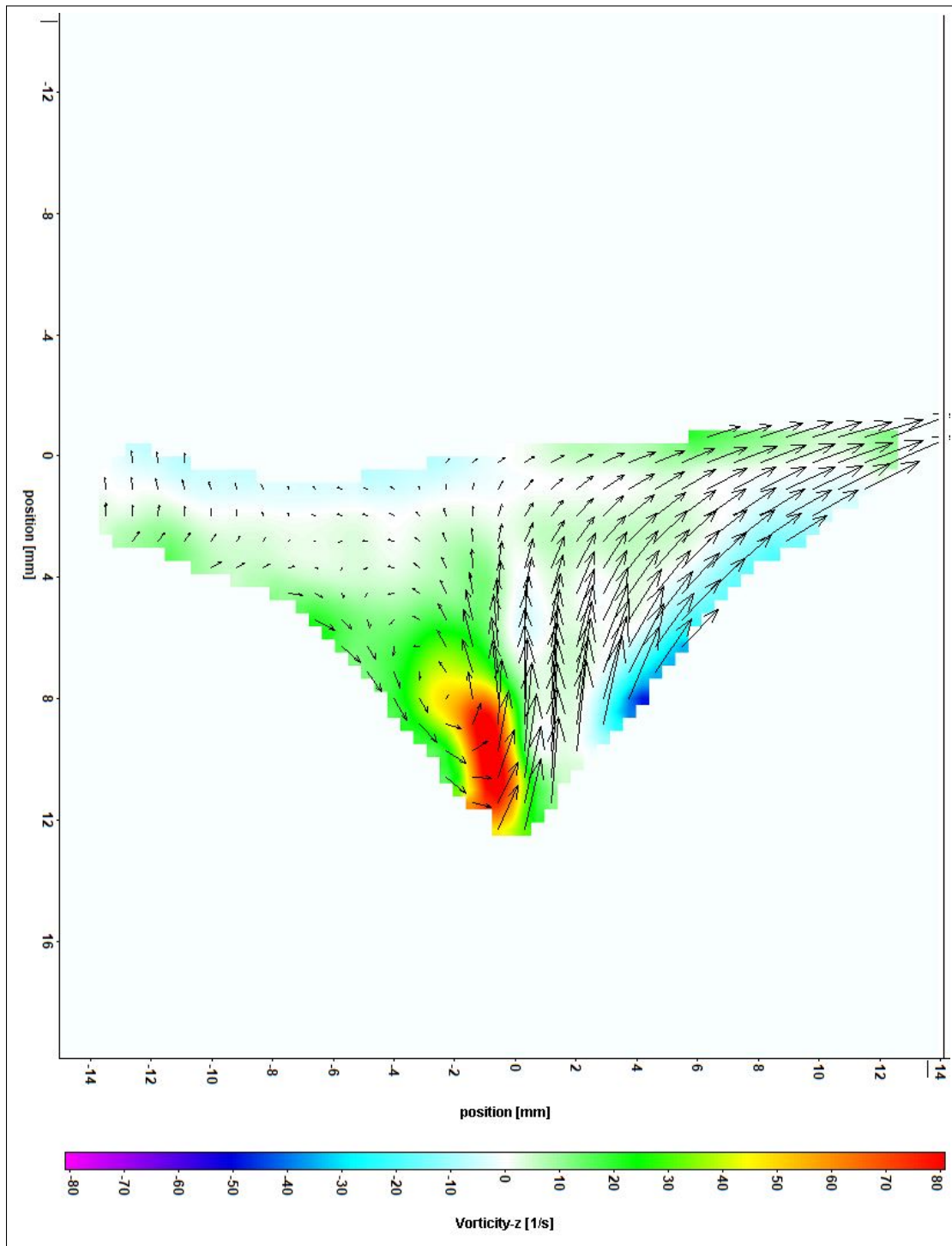


Figure 3.6: 1 rad/s After Completing Extension

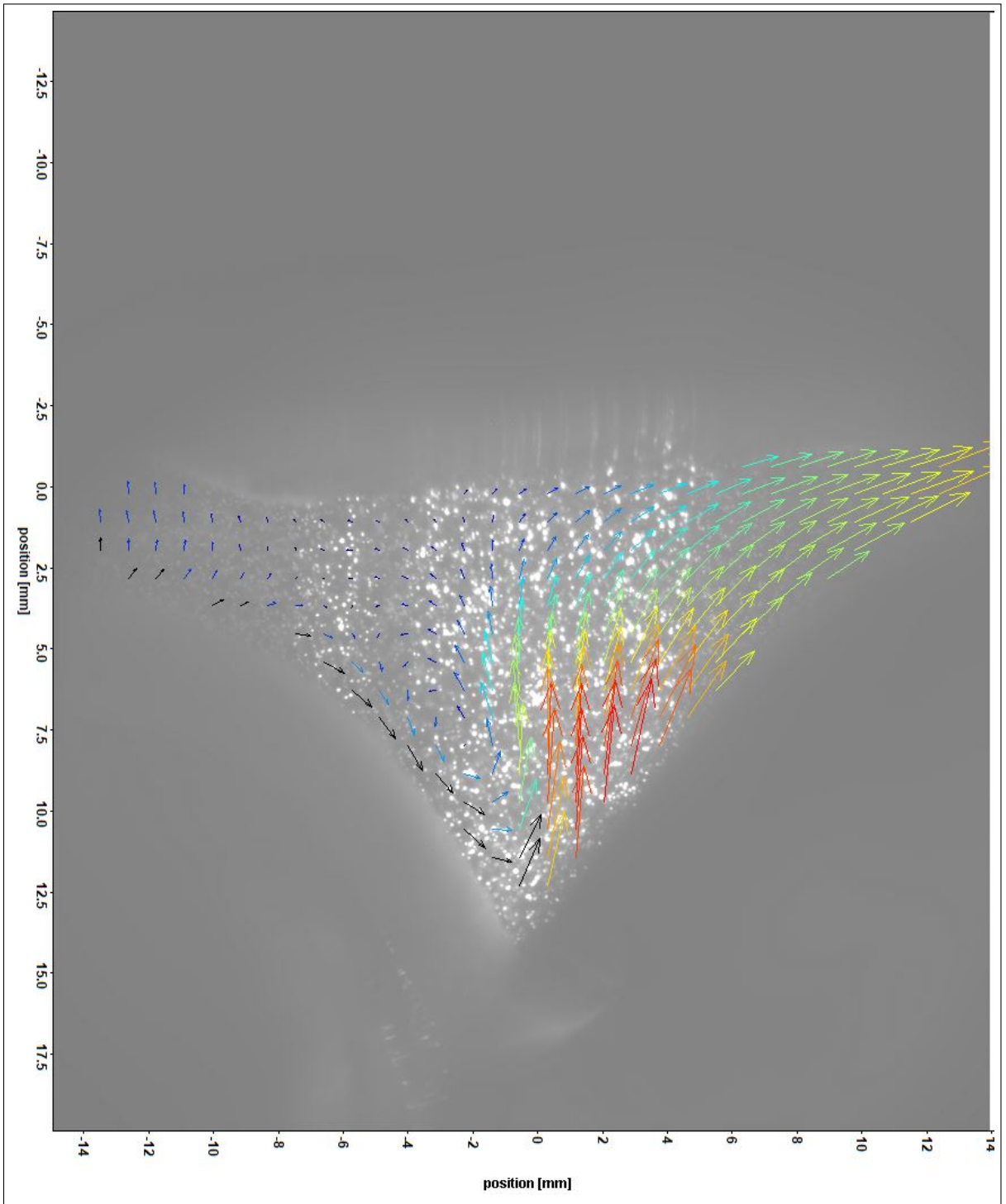


Figure 3.7: 1 rad/s After Completing Extension Over Raw Image

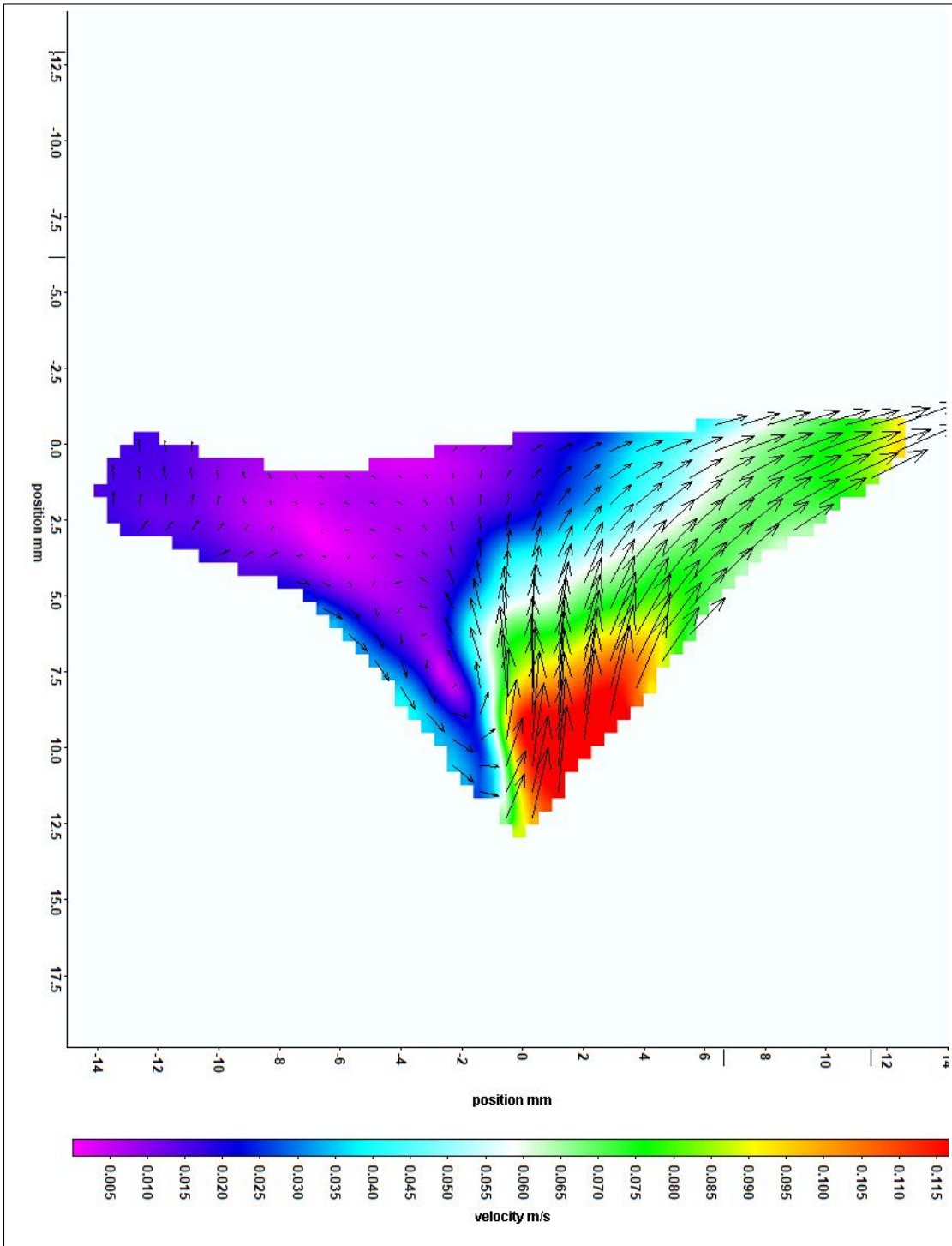


Figure 3.8: 1 rad/s After Completing Extension Velocity Only

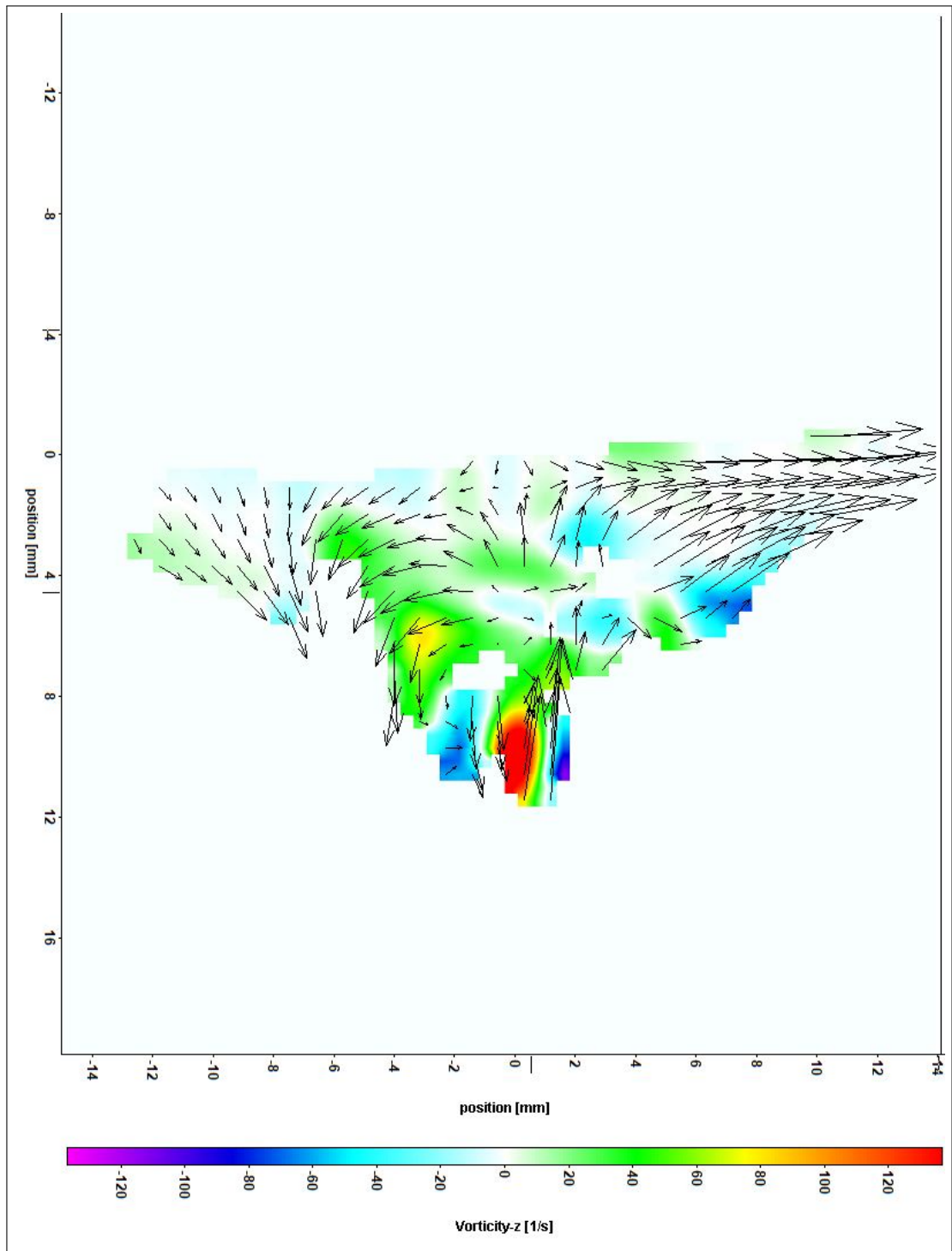


Figure 3.9: 3 rad/s Before Completing Extension

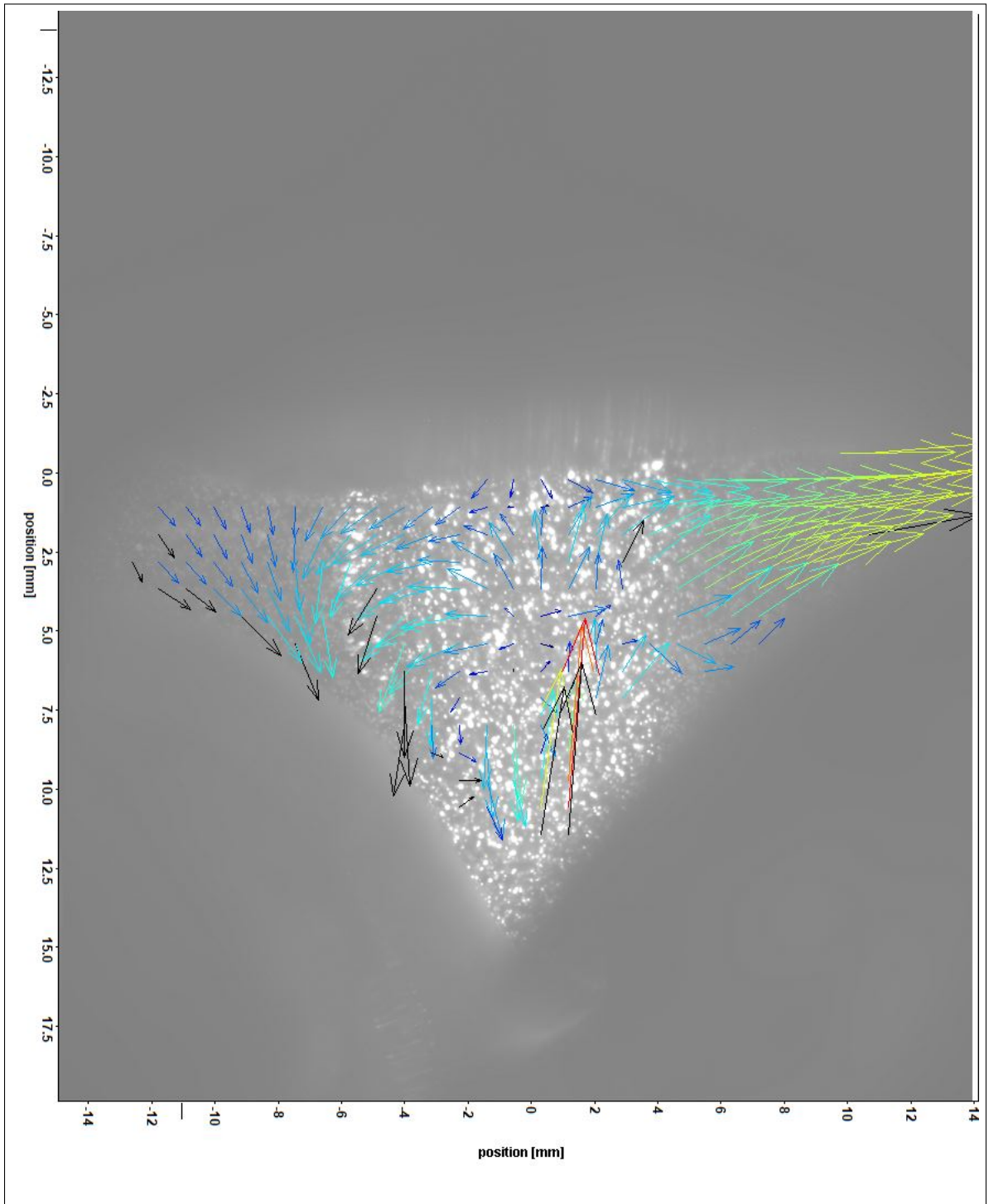


Figure 3.10: 3 rad/s Before Completing Extension Over Raw Image

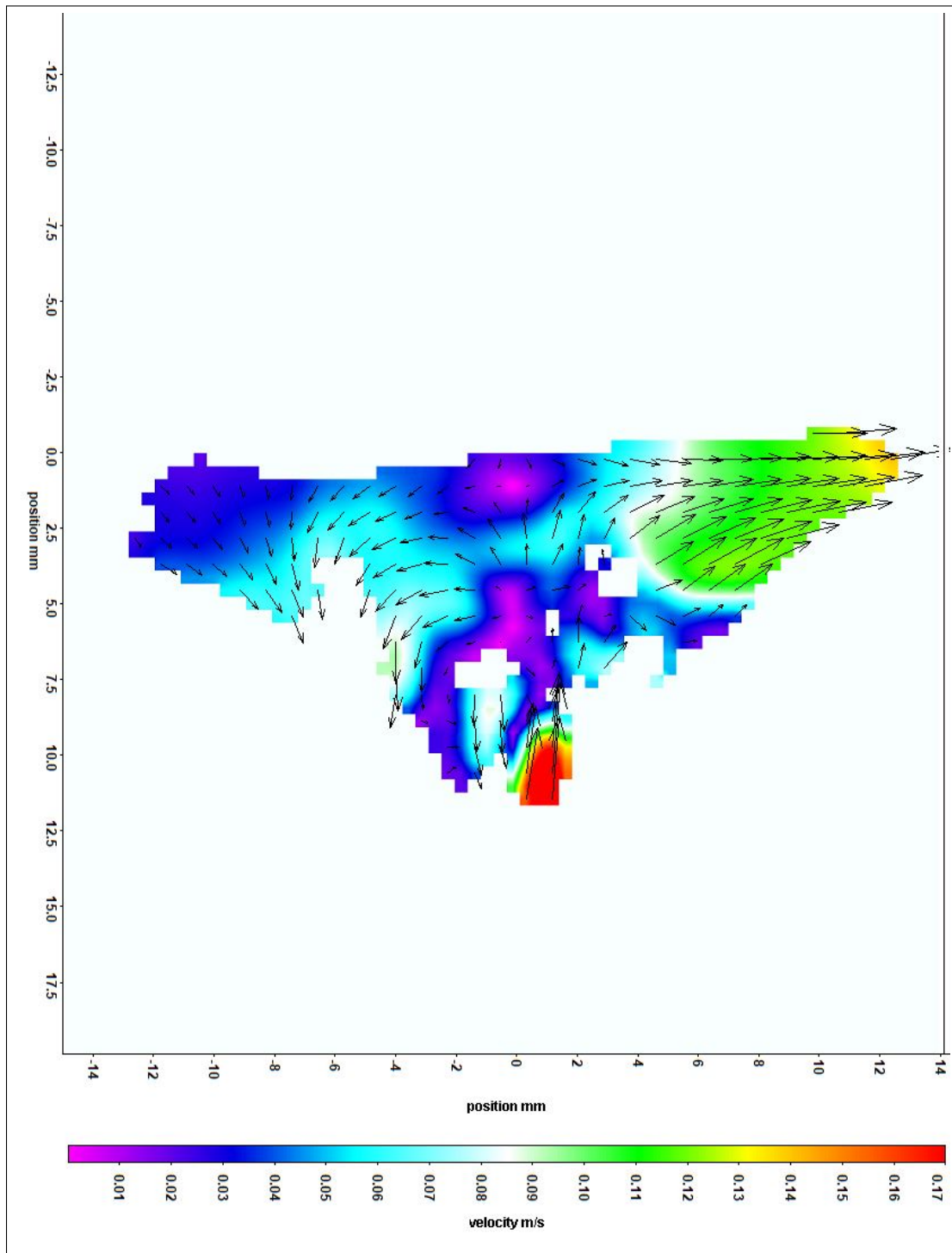


Figure 3.11: 3 rad/s Before Completing Extension Velocity Only

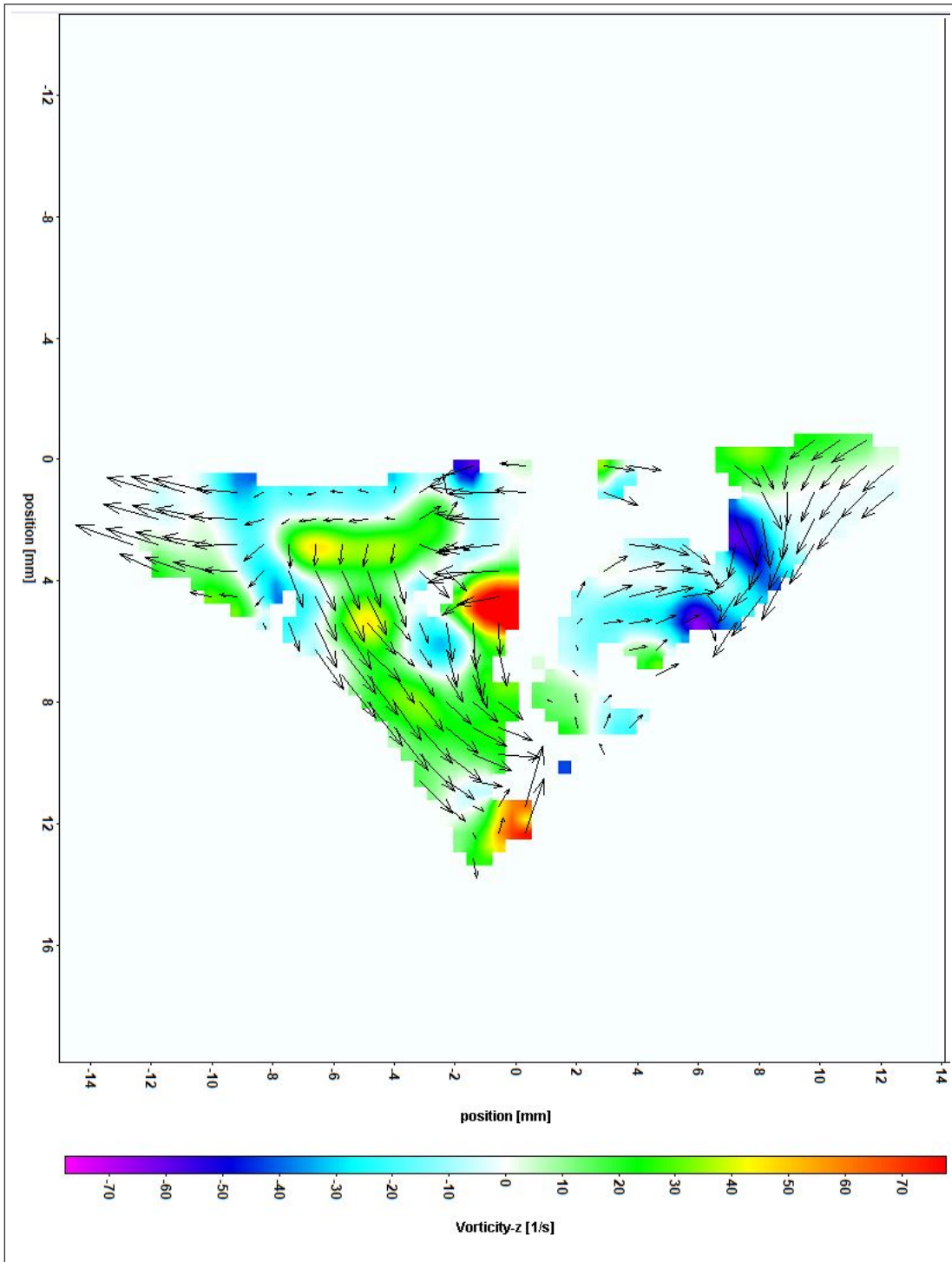


Figure 3.12: 3 rad/s After Completing Extension

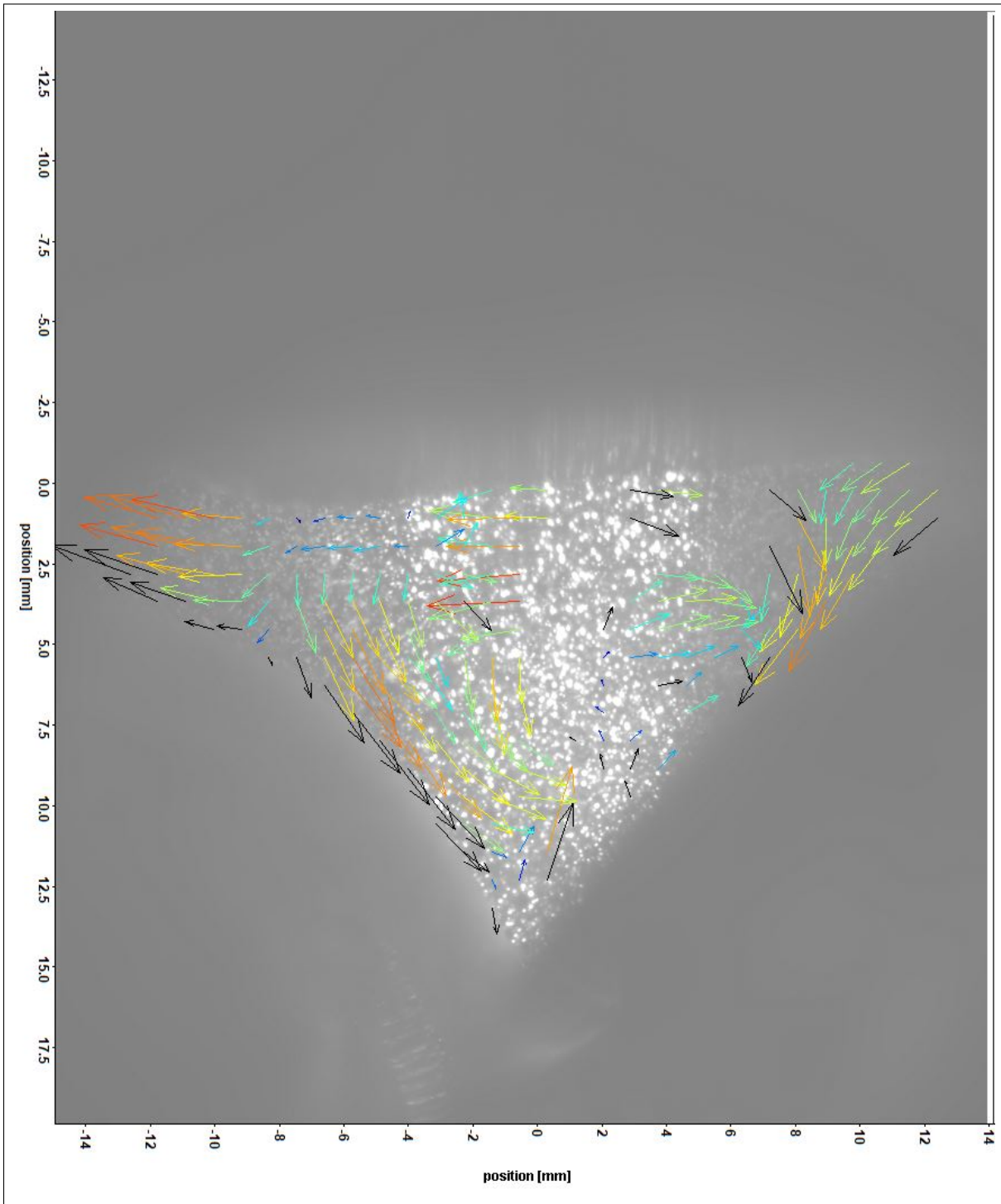


Figure 3.13: 3 rad/s After Completing Extension Over Raw Image

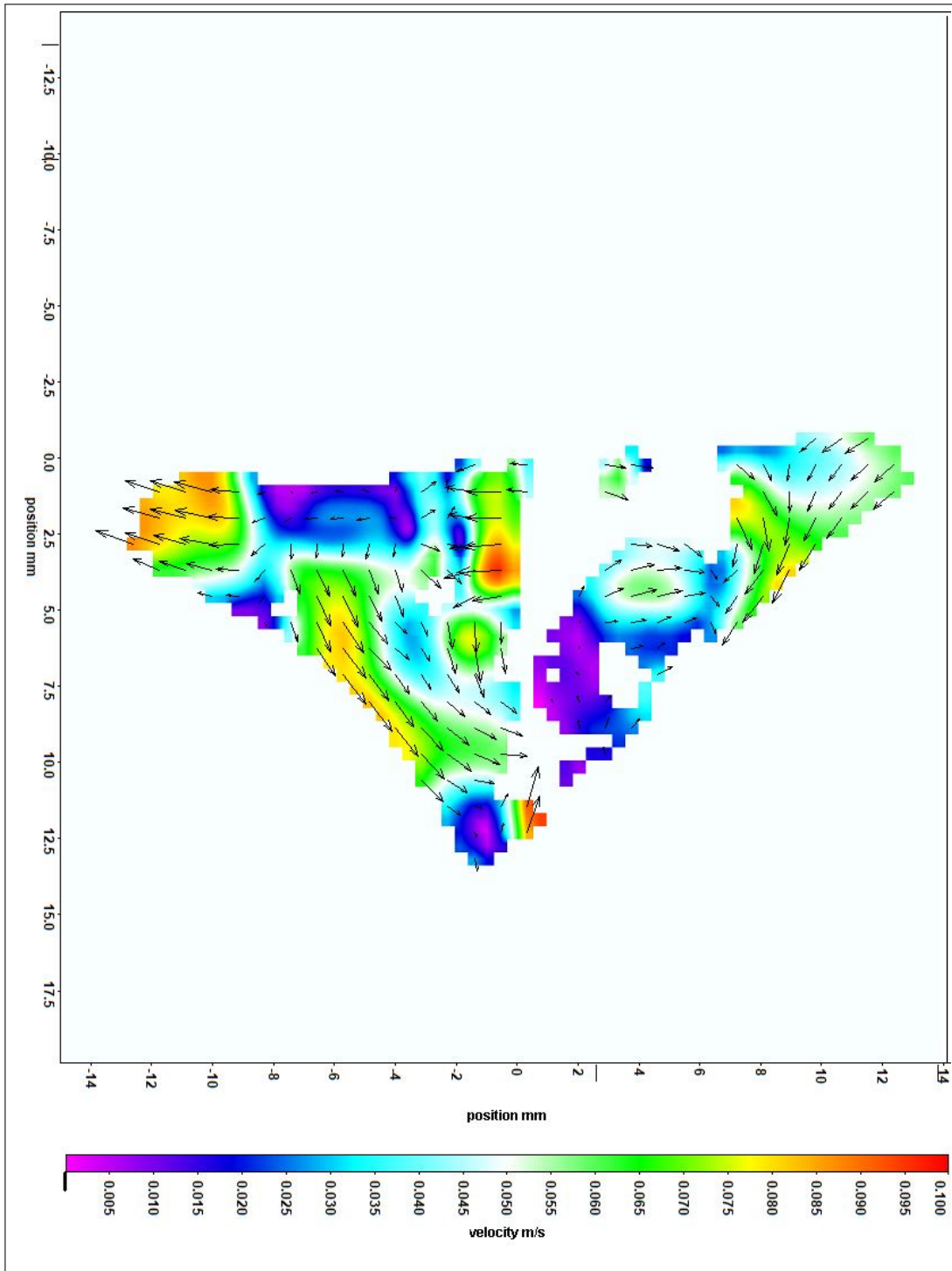


Figure 3.14: 3 rad/s After Completing Extension Velocity Only

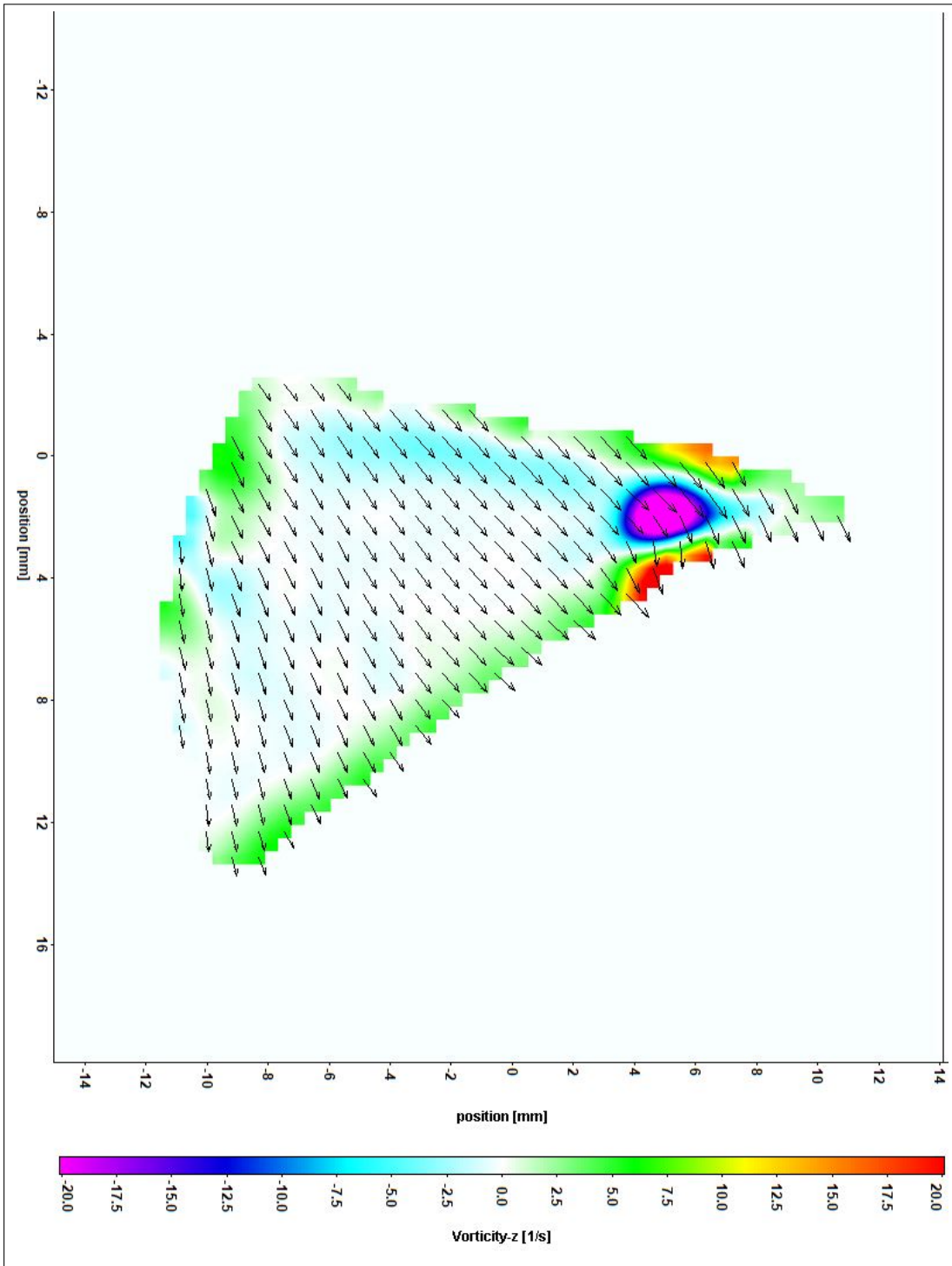


Figure 3.15: 1 rad/s Before Completing Flexion

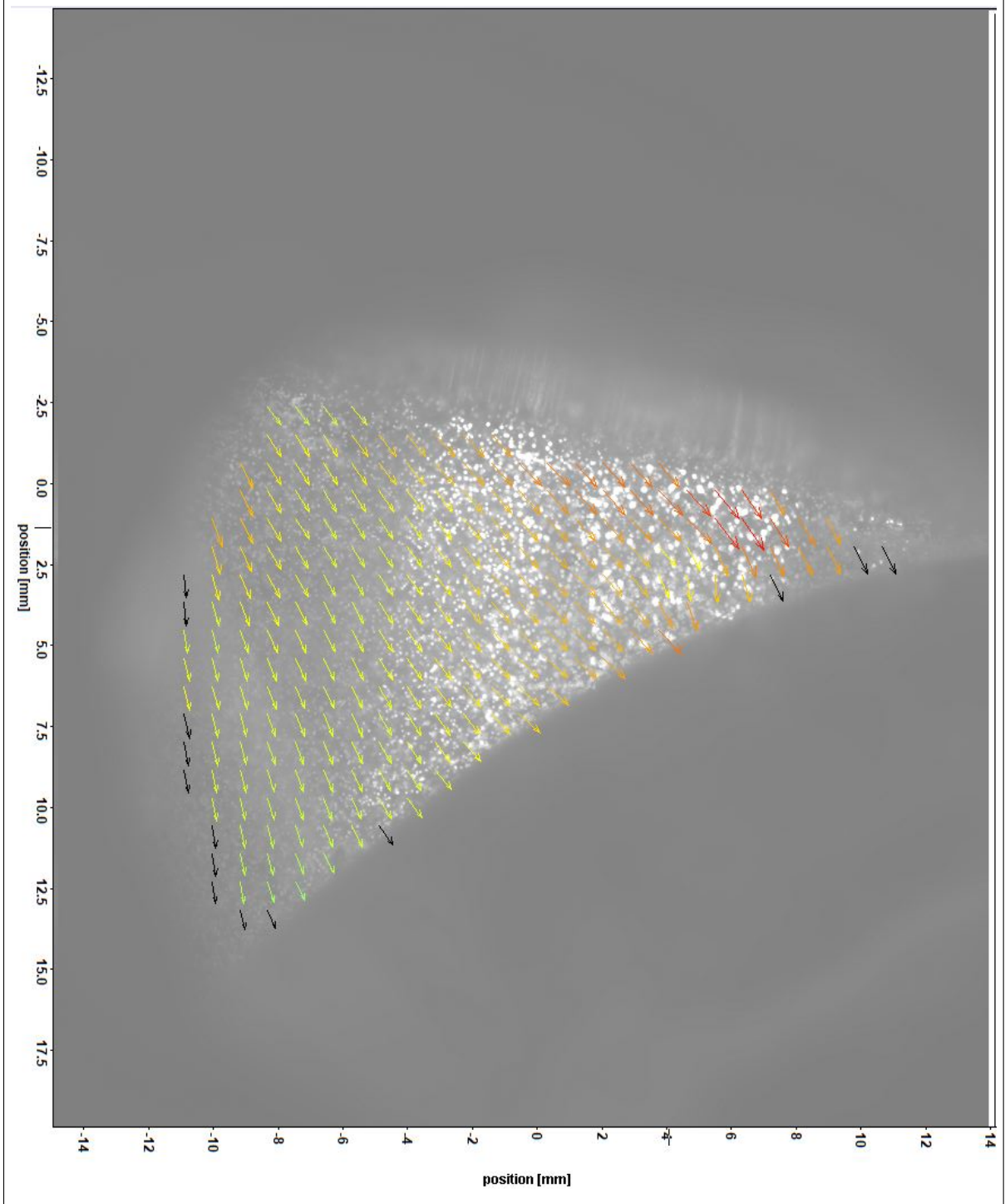


Figure 3.16: 1 rad/s Before Completing Flexion Over Raw Image

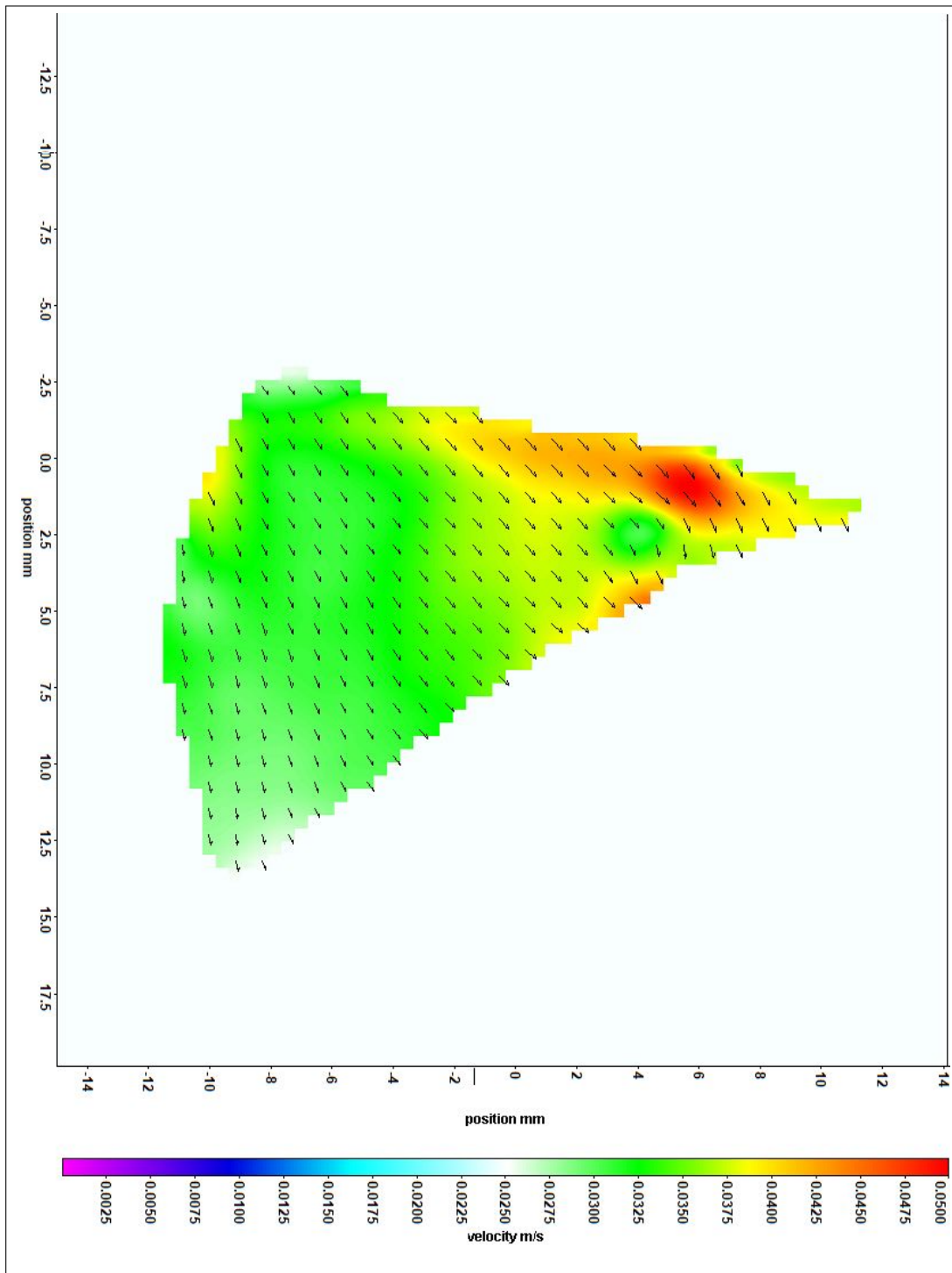


Figure 3.17: 1 rad/s Before Completing Flexion Velocity Only

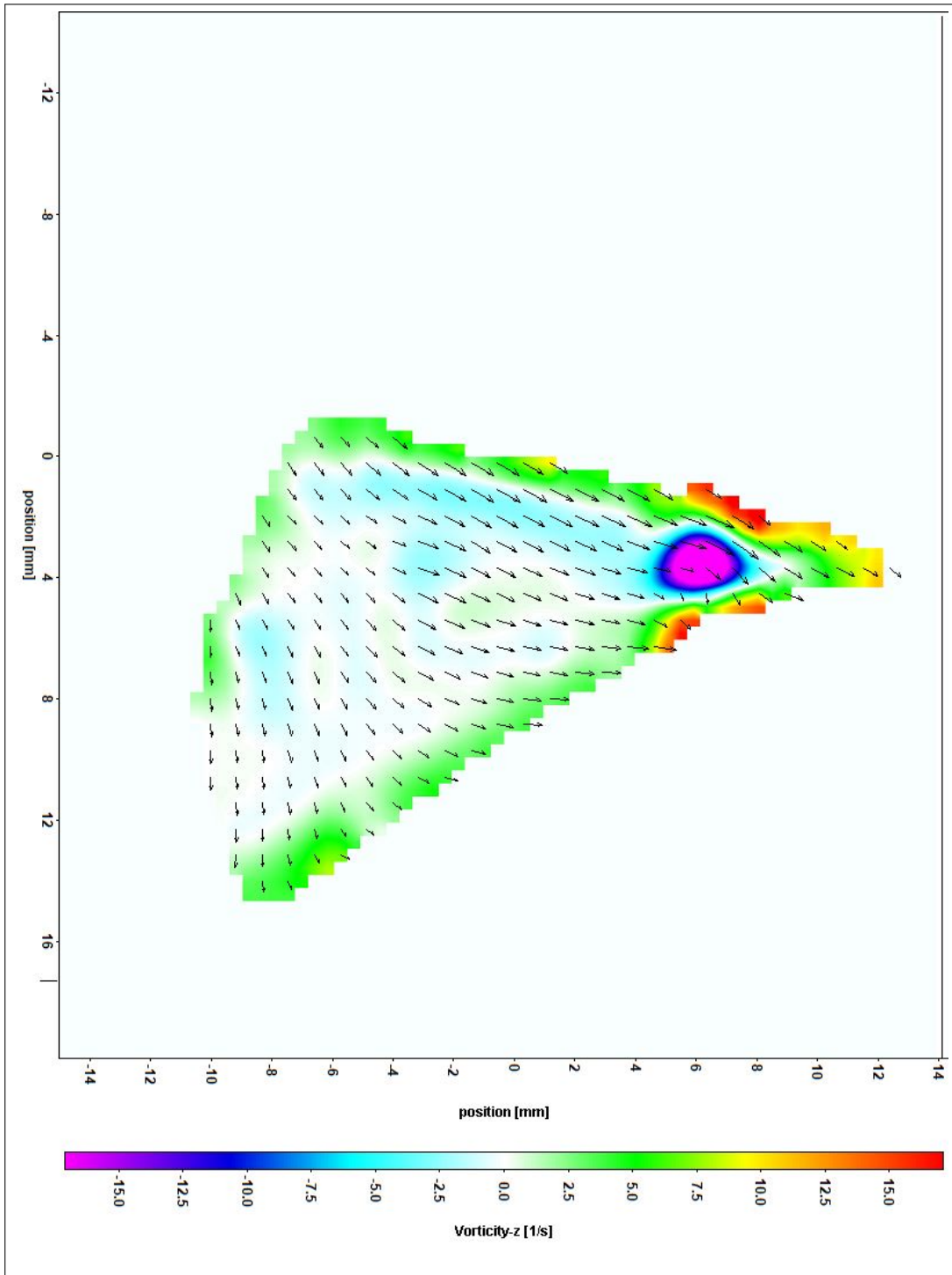


Figure 3.18: 1 rad/s After Completing Flexion

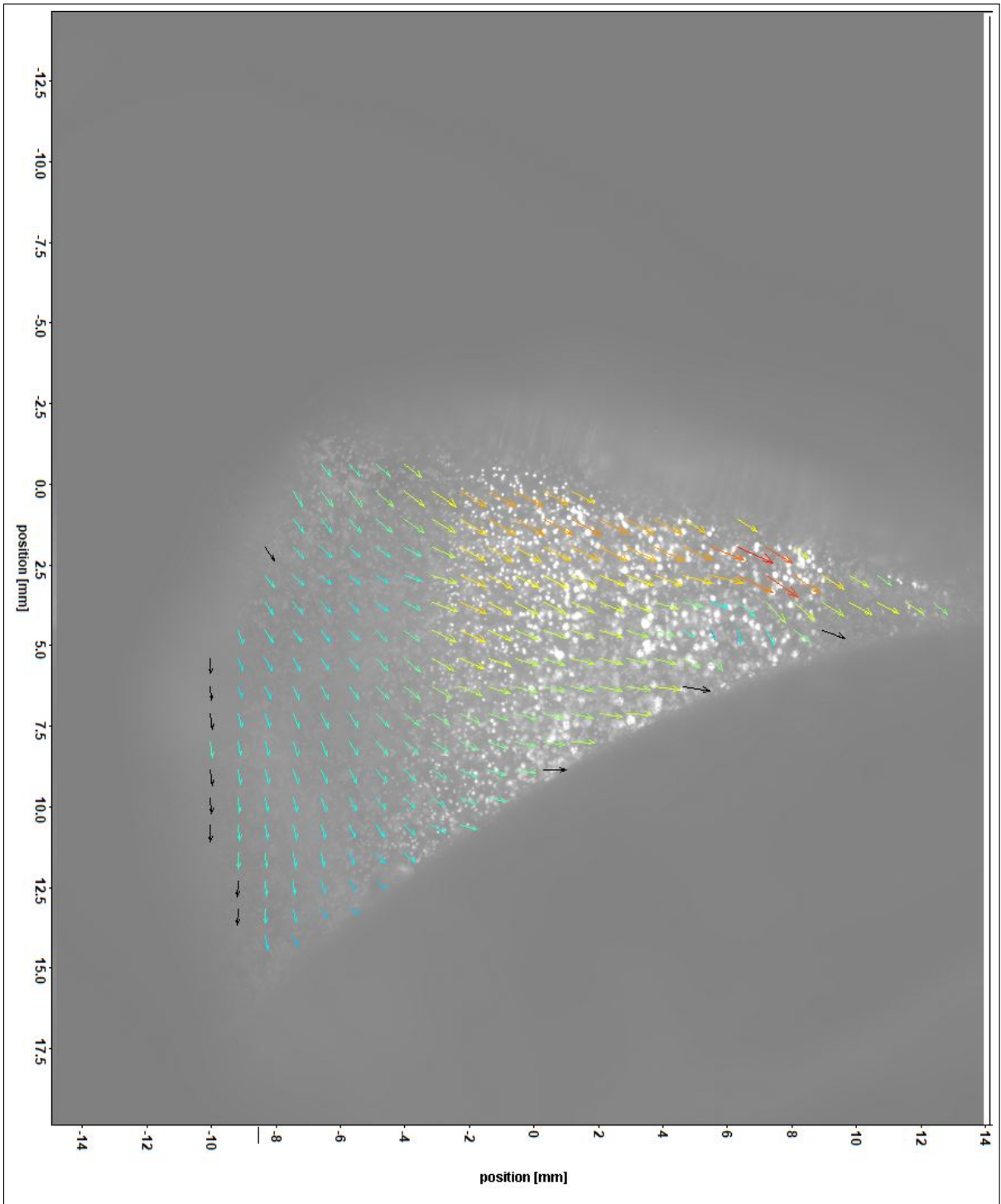


Figure 3.19: 1 rad/s After Completing Flexion Over Raw Image

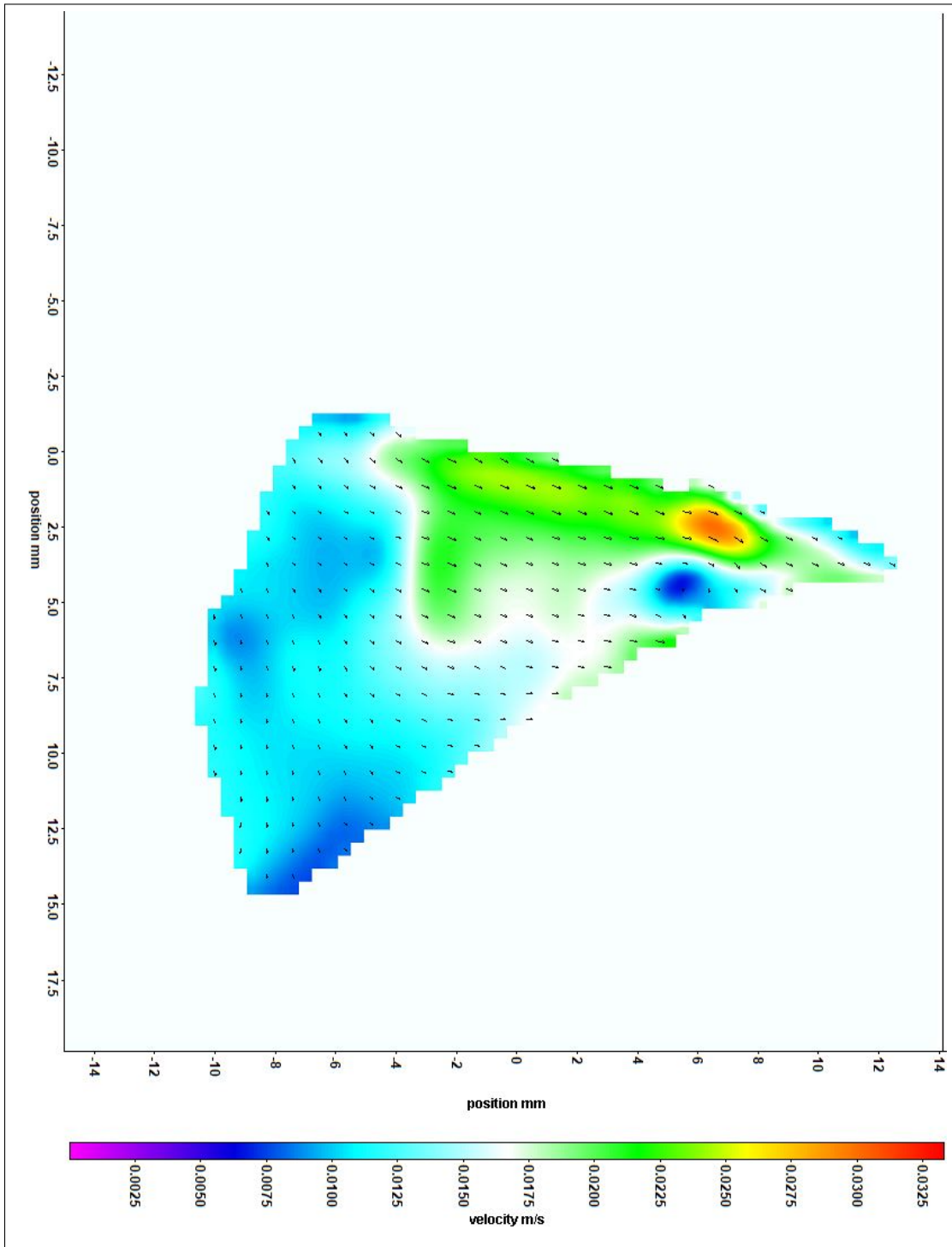


Figure 3.20: 1 rad/s After Completing Flexion Velocity Only

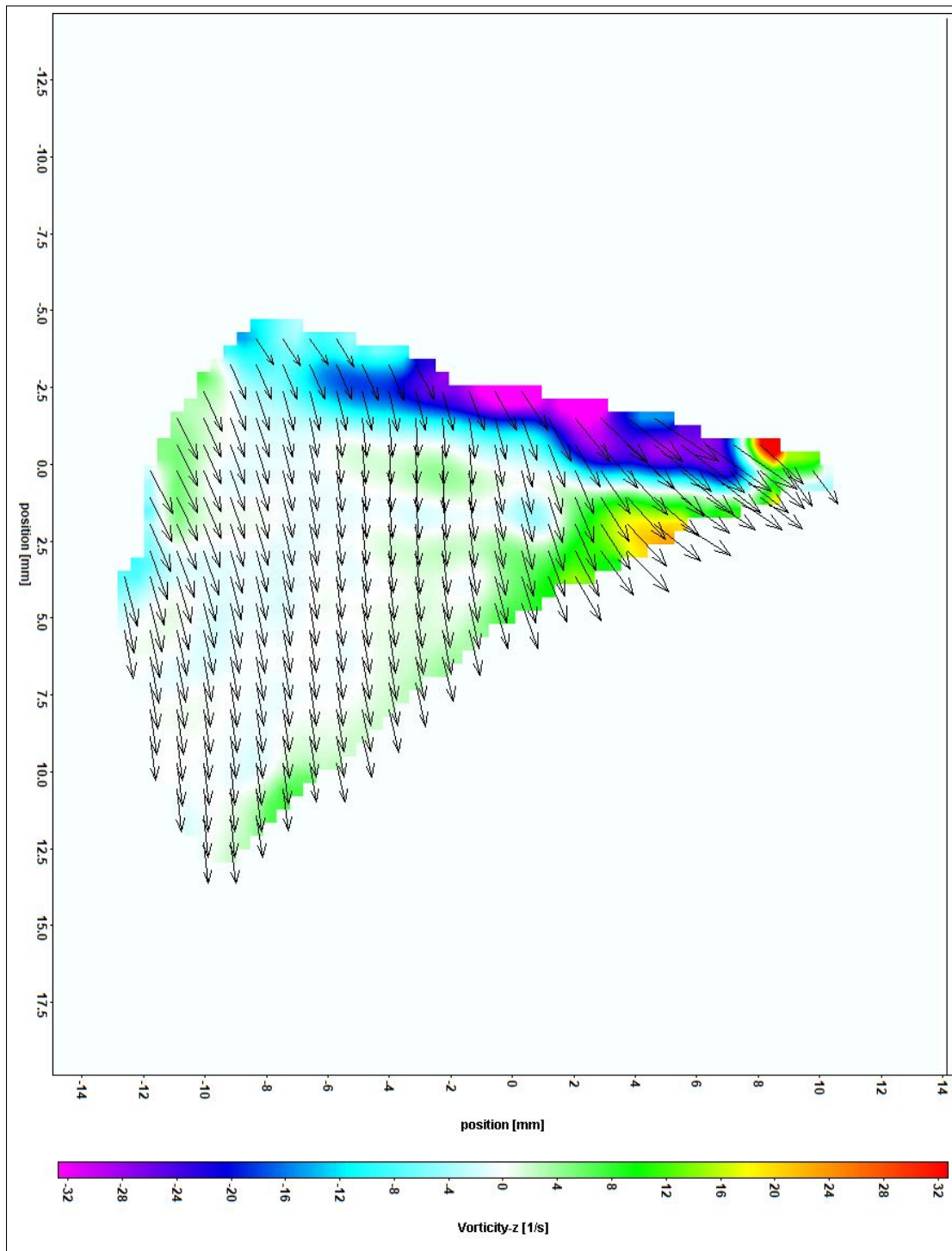


Figure 3.21: 3 rad/s Before Completing Flexion

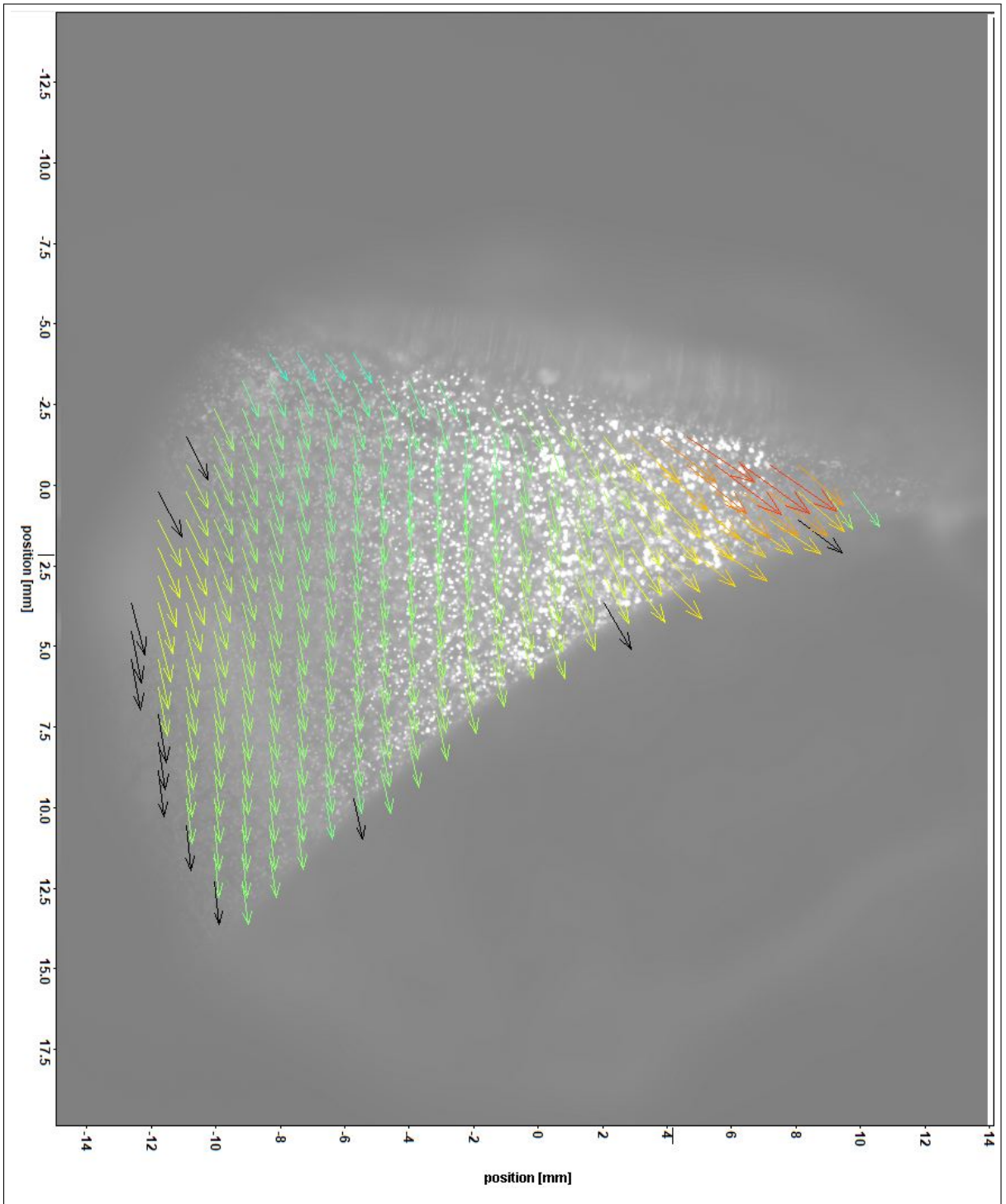


Figure 3.22: 3 rad/s Before Completing Flexion Over Raw Image

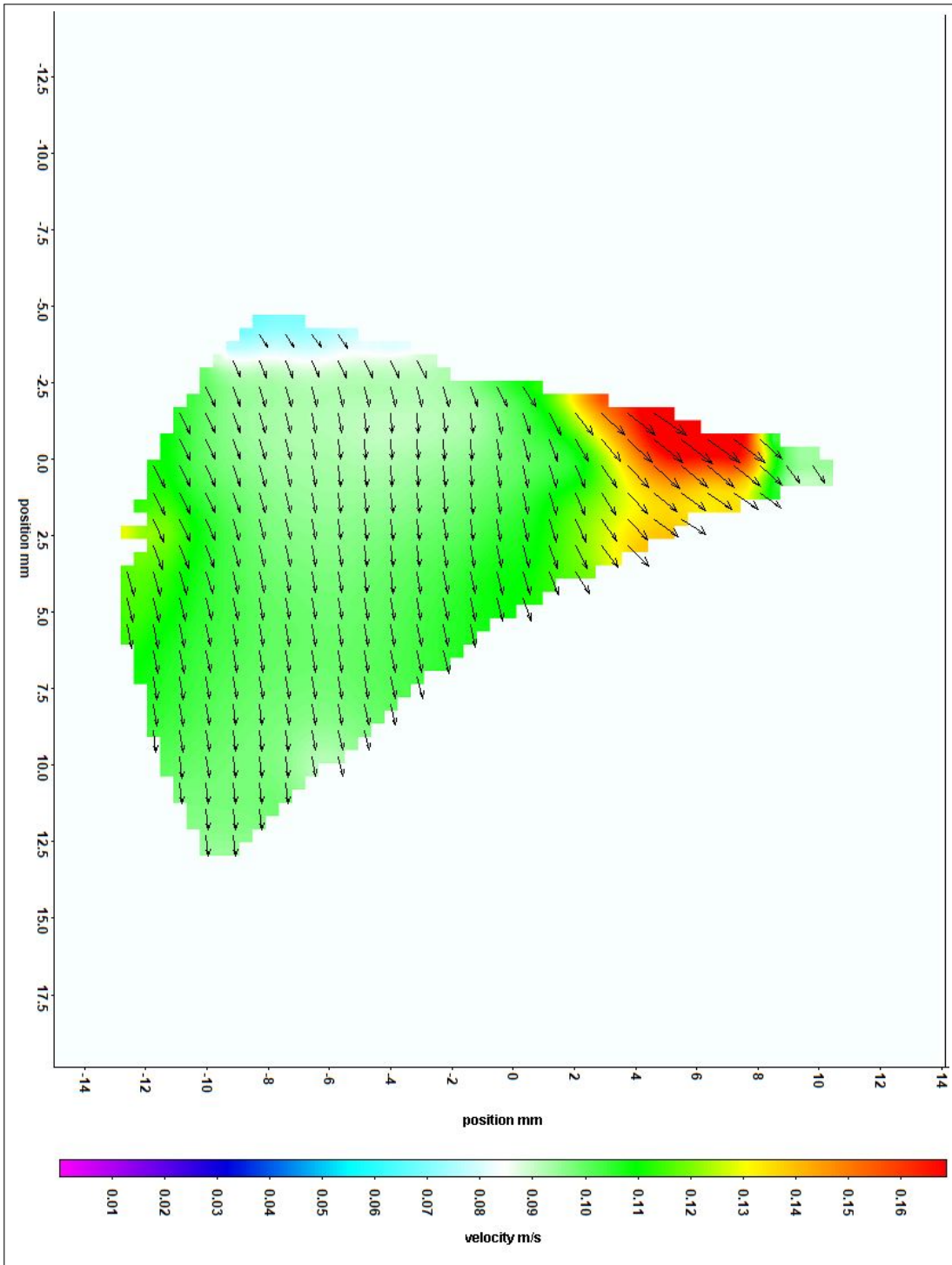


Figure 3.23: 3 rad/s Before Completing Flexion Velocity Only

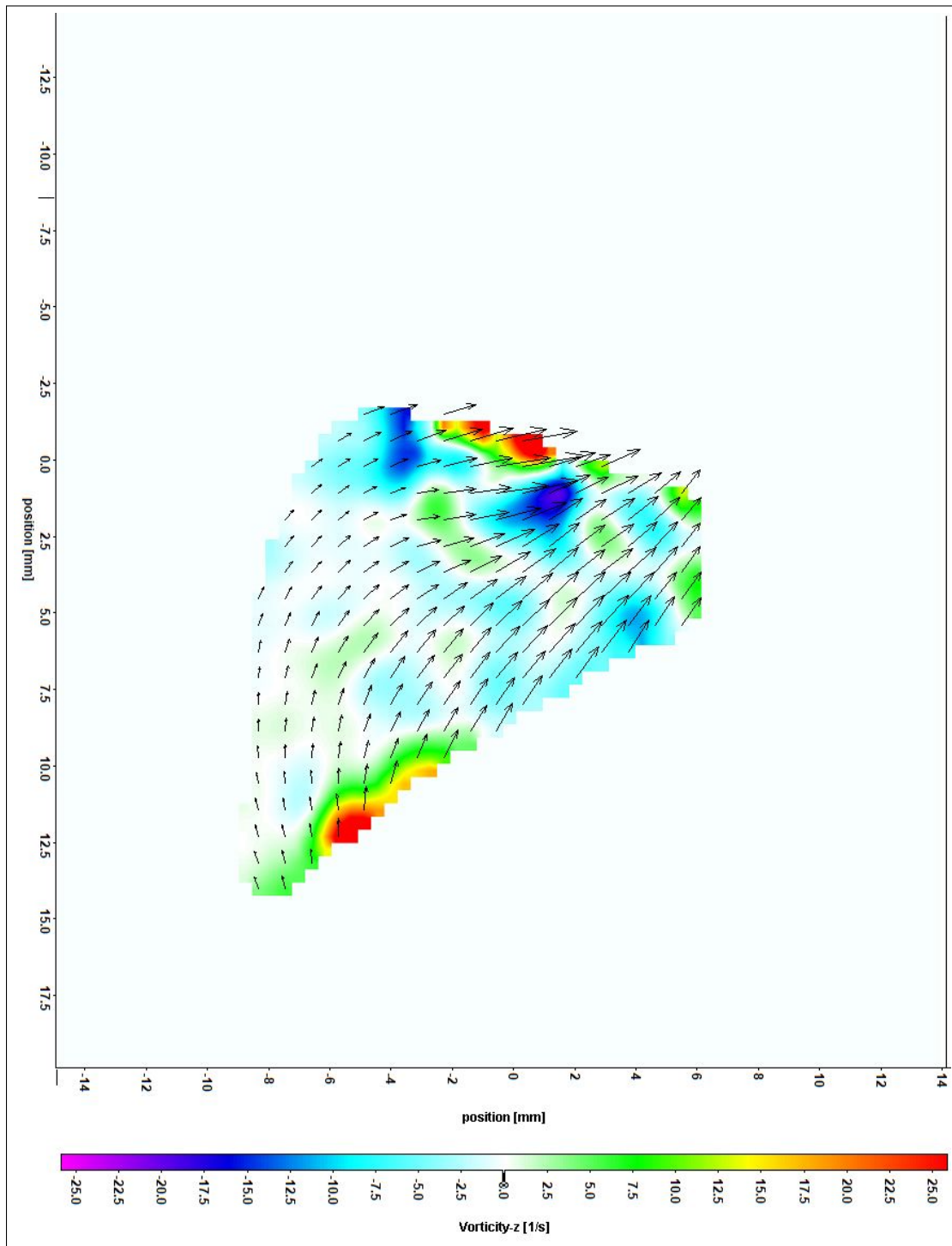


Figure 3.24: 3 rad/s After Completing Flexion

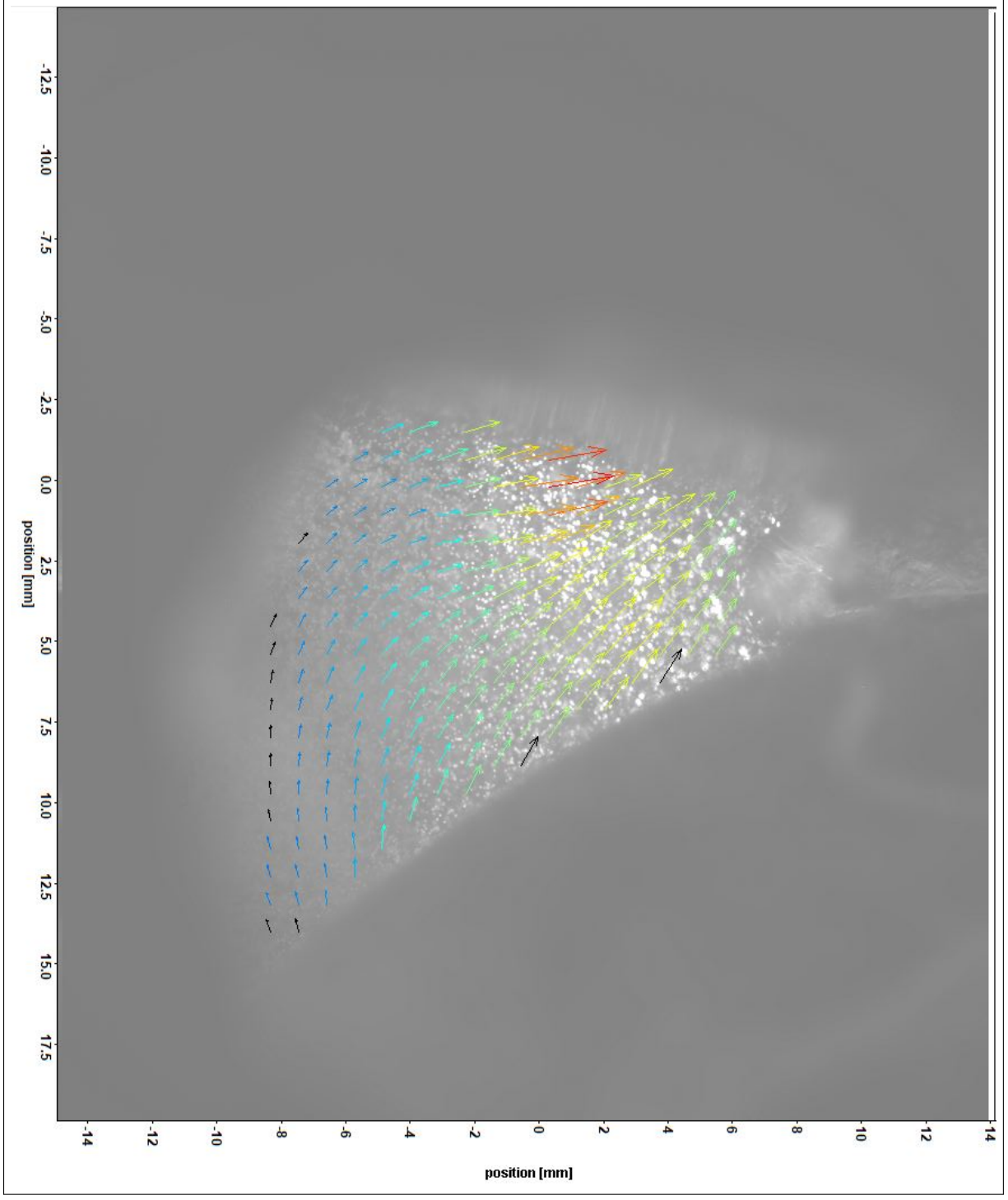


Figure 3.25: 3 rad/s After Completing Flexion Over Raw Image

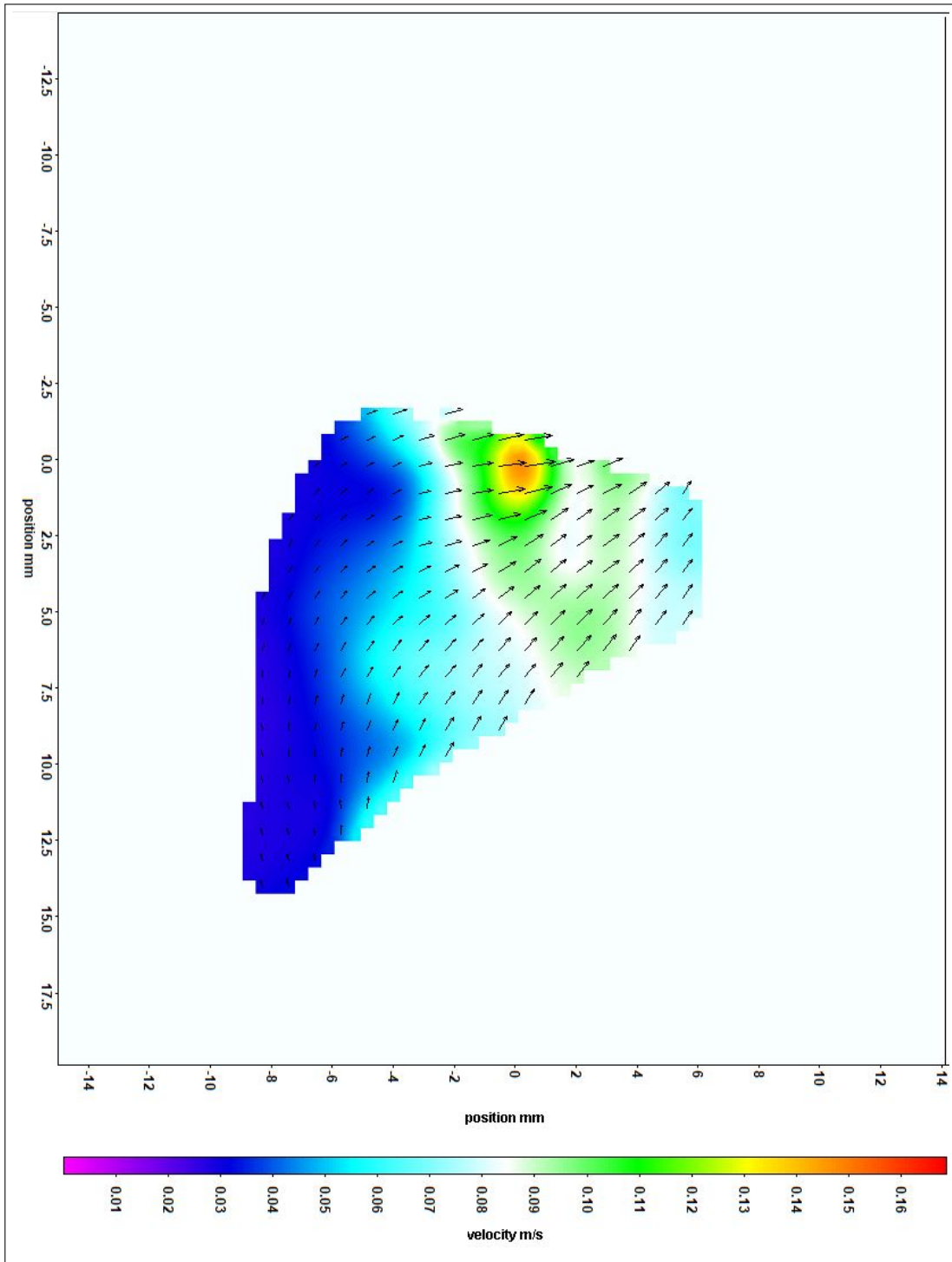


Figure 3.26: rad/s After Completing Flexion Velocity Only

Each of the data points were then analyzed after the image processing to determine a rough direction of flow as well as a general direction of vorticity. The analysis can be found in the next section.

# 4

## Analysis

### 4.1 EXTENSION

Each image in the data section of this report was analyzed and Table 4.1 below shows a summary of the velocity and vorticity for each of the cases tested for extension of the knee. Each pair of images was compared to one another in an attempt to see what happens right before a full extension is reached and what happens when the knee stops extending.

Rotational Speed	Before/after completion	Peak Velocity (m/s)	Average Velocity at bearing surface (m/s)	Velocity Direction	Max Vorticity (1/s)	Vorticity Direction
1 rad/s	Before	.105	.08	Towards Patella/away from the joint vertically	25	negligible
1 rad/s	After	.120	.08	Towards the patella/femur connection	80	CCW at the tibia/femur connection
3 rad/s	Before	.170	.1	No clear pattern. Either directly north or back towards the tibia/femur connection	125	CCW at inner most tibia/femur connection
3 rad/s	After	.085	.06	No clear pattern	65	generally CCW all over

Table 4.1: Extension Data

Figures 3.3 through 3.8 indicate that while in motion with a rotational speed of 1 rad/s, or just before stopping, the majority of the fluid is moving outwards towards the patella. The fluid particles closest to the tibia and femur are moving faster at roughly .105 m/s while the fluid towards the patella is moving outwards closer to .03 m/s. After the initial extension is stopped, we see that the areas of vorticity continue to grow and the general fluid movement is outwards towards the patella and up towards the femur. The velocities of the fluid near the tibia and femur, where the more turbulent areas are, speed up to approximately .12 m/s whereas the rest of the fluid tends to slow down when the extension is completed.

The 3 rad/s extension data points came out less clear than the 1 rad/s extension testing. Figures 3.9 through 3.14 show the same moments previously described. It is difficult to analyze, but it is noted that the vortical motion is in the same region as the 1 rad/s data points. It seems that the motion was so quick and forceful that the entire fluid sack was in rotation. The peak velocity at the end of motion was .17 m/s. After stopping, the fluid towards the top of the sack traveled towards the inner knee while the fluid towards the inner knee flowed downwards and out towards the bottom of the patella. The abrupt stop might have caused the scramble of the fluid particles. This is interesting as it leads to questioning the impact of hard stops on the knee. This data is initially unclear but helps to justify further study.

## 4.2 FLEXION

Each image in the data section of this report was analyzed and Table 4.2 below shows a summary of the velocity and vorticity for each of the cases tested for flexion of the knee. Each pair of images was compared to one another in an attempt to see what happens right before a full extension is reached and what happens when the knee stops extending.

Rotational Speed	Before/after completion	Peak Velocity (m/s)	Average Velocity at bearing surface (m/s)	Velocity Direction	Max Vorticity (1/s)	Vorticity	Direction
1 rad/s	Before	.047	.035	Towards the femur	20	negligible	
1 rad/s	After	.025	.015	Towards the femur	16	negligible	
3 rad/s	Before	.3	.11	Towards the patella and the patella/femur connection	25	negligible	
3 rad/s	After	.085	.065	Towards the patella and the patella/femur connection	20	negligible	

Table 4.2: Flexion Data

The next set of data points collected was the 1 rad/s flexion of the knee. As a whole, the fluid movement was rather simple during this set of points. The fluid all flowed towards the femur at roughly .035 m/s right before stopping. The top portion of the viewing triangle had a small amount of vorticity. After stopping, the general direction moved towards the upper patella and femur connection. The fluid towards the bottom of the sack slows down quickly and seems to move away from the patella. The general direction of the fluid is the opposite when compared to the 1 rad/s extension analysis. The fluid flow continues to move and induce different directions of vorticity even after the actuation has ended. Roughly 6 frames after stopping, the vorticity map of the fluid shows opposite directions when compared to the initial stop towards the bottom of the viewing triangle. Figure 4.1 below shows this case.

The fast flexion movement drastically changes at the end of flexion. Before the end of the fast flexion motion, the fluid movement is very similar to the slow flexion movement. The difference is, once the flexion ends, the fluid abruptly switches its direction and heads towards the patella instead for a short time. This general flow is actually the same as the slow extension data which is intuitively backwards. After further investigation, the general direction of the flow goes from towards the center of patella to away from the patella after a few frames. It seems that the abrupt stop on the joints reverses the fluid motion for a split second before continuing in its initial direction. This is a similar assumption to the trivial data captured in the fast extension portion of the testing.

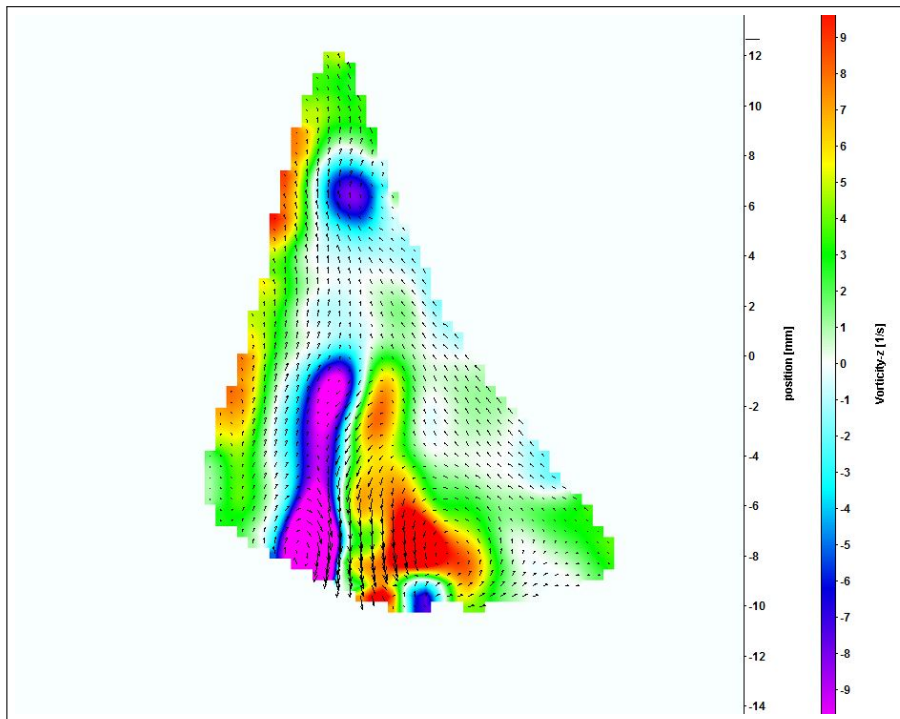


Figure 4.1: 1 rad/s Flexion Vorticity

# 5

## Conclusion

The goal of this investigation was to analyze the feasibility and capability of using Particle Image Velocimetry technology on joints such as the human knee. This initial study proved successful in being able to see the fluid movement inside of a joint with the proper test set-up. The PIV hardware and software was able to be navigated to meet the needs of the investigation. Data was collected and able to be analyzed to discover some interesting concepts that can be investigated further. The

general direction and velocities of fluid flow in the knee for each of the 4 cases tested were noted and the discoveries of some possible boundaries were as well. It seems that with the current set-up, flexion/extension at too fast of a rate will create difficult data to analyze. It was interesting to see what happened at faster rates of flexion/extension and these difficult data points could be an asset to working with joint recovery therapy and the correct methods to strengthen and exercise the area of interest.

The data collected so far warrants additional testing, but with a more robust and sturdy model than used previously. Additionally, actual synovial fluid should be used in place of water to help better simulate the actual fluid motion now that we have proven feasibility. Water and synovial fluid have different properties and may act differently under the motion of flexion and extension in a joint. The final element of the model that could be altered for a more accurate representation of the knee movement would be a more dynamically correct method to control the extension/flexion. The elastic bands holding the bones together work for a rough model but a more accurate form of movement should be substituted in the future. An article was found that explains the movement of the human knee and how best to mechanically simulate it. A 4-bar linkage system can be built to create the Burmester curve in the knee when actuated that will help to keep the ligament lengths the same during flexion/extension [7]. The Burmester curve is known to be the most important biomechanical principal considered when working with ligament injuries and surgeries [7]. This curve can be seen in the image below and is recommended for consideration when furthering the investigation on the fluid flow in the knee.

The information collected from this study proves that Particle Image Velocimetry technology can be

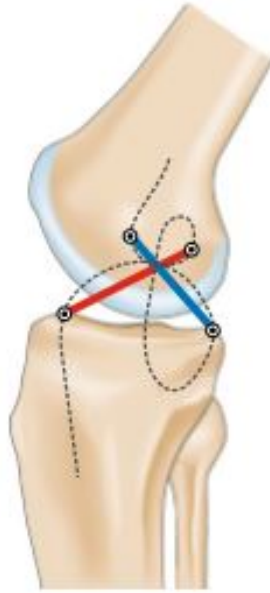


**Figure 5.1:** Illustration of the Burmester curve and four-bar linkage system [7]

used in the biomechanical field with specific use in the investigation of fluid velocities in synovial joints. Further investigation will be an important tool to verifying a Computational Fluid Dynamics model for any joint. CFD models may have been attempted but there was no accurate method of checking the model against an actual system. A working CFD model can and will be extremely useful with improving replacement materials, recovery methods, and surgical techniques in various joints. Being able to predict accurately how different exercises will affect knee replacements is vital in improving the rates of successful recoveries.

# References

- [1] (2016). Fluid film bearings.
- [2] Agrawal, K., Saxena, R., Sahay, K., Arvind, A., Dave, P., & Dogra, T. (1995). Biochemical kinetics in articular cartilage and synovial fluid. In *Engineering in Medicine and Biology Society, 1995 and 14th Conference of the Biomedical Engineering Society of India. An International Meeting, Proceedings of the First Regional Conference., IEEE* (pp. 3–93).: IEEE.
- [3] Budynas, R. G., Nisbett, J. K., & Shigley, J. E. (2015). *Shigleys mechanical engineering design*. McGraw-Hill Education.
- [4] Cao, X., Liu, J., Jiang, N., & Chen, Q. (2014). Particle image velocimetry measurement of indoor airflow field: A review of the technologies and applications. 69, 367–380.
- [5] Gutierrez-Miravete, P. E. (2012). Lubrication.
- [6] Harnoy, A. (2002). *Bearing Design in Machinery: Engineering Tribology and Lubrication*. Dekker Mechanical Engineering. Taylor & Francis.
- [7] Hirschmann, M. T. & Müller, W. (2015). Complex function of the knee joint: the current understanding of the knee. *Knee Surgery, Sports Traumatology, Arthroscopy*, 23(10), 2780–2788.
- [8] Hoffman, M. (2016). Picture of the knee.
- [9] Jeffress, D. & Walker, J. (2017). What does ”tibial tuberosity” mean?
- [10] Jin, Z., Medley, J., & Dowson, D. (2003). Fluid film lubrication in artificial hip joints. *Tribology Series*, 41, 237–256.
- [11] Johnson, R. (2016). *Handbook of Fluid Dynamics, Second Edition*. CRC Press.
- [12] Katta, J., Jin, Z., Ingham, E., & Fisher, J. (2009). Effect of nominal stress on the long term friction, deformation and wear of native and glycosaminoglycan deficient articular cartilage. *Osteoarthritis and Cartilage*, 17(5), 662–668.

- [13] Kienle, S., Boettcher, K., Wiegleb, L., Urban, J., Burgkart, R., Lieleg, O., & Hugel, T. (2015). Comparison of friction and wear of articular cartilage on different length scales. *Journal of biomechanics*, 48(12), 3052–3058.
- [14] Knudson, D. (2003). *Fundamentals of biomechanics*. Kluwer academic.
- [15] Kumar, P. & Kandadai, R. (2015). Finite element modeling of human knee joint - meniscus under compressive load. *International Journal of mechanical and production engineering*, 3(3).
- [16] Miller, M. & Thompson, S. (2015). *Miller's Review of Orthopaedics E-Book*. Elsevier Health Sciences.
- [17] Ombregt, L. (2013). *A System of Orthopaedic Medicine - E-Book*. Elsevier Health Sciences.
- [18] Patten, E. W., Van Citters, D., Ries, M. D., & Pruitt, L. A. (2013). Wear of uhmwpe from sliding, rolling, and rotation in a multidirectional tribo-system. *Wear*, 304(1), 60–66.
- [19] Rao, T., Rani, A., Nagarajan, T., & Hashim, F. (2014). Analysis of couple stress fluid lubricated partially textured slip slider and journal bearing using narrow groove theory. *Tribology International*, 69, 1–9.
- [20] Stewart, T., Williams, S., Tipper, J., Ingham, E., Stone, M., & Fisher, J. (2003). Advances in simulator testing of orthopaedic joint prostheses. *Tribology Series*, 41, 291–296.
- [21] Strandring, S. (2009). *Gray's Anatomy - The anatomical Basis of Clinical Practice*. 40 edition.



**T**HIS THESIS WAS TYPESET using  $\LaTeX$ , originally developed by Leslie Lamport and based on Donald Knuth's  $\TeX$ . The body text is set in 11 point Egenolff-Berner Garamond, a revival of Claude Garamont's humanist typeface. The above illustration, *Science Experiment 02*, was created by Ben Schlitter and released under [CC BY-NC-ND 3.0](#). A template that can be used to format a PhD dissertation with this look & feel has been released under the permissive AGPL license, and can be found online at [github.com/suchow/Dissertate](https://github.com/suchow/Dissertate) or from its lead author, Jordan Suchow, at [suchow@post.harvard.edu](mailto:suchow@post.harvard.edu).